THE PROCEEDINGS OF THE PHYSICAL SOCIETY

Section B

Vol. 65, Part 4 1 April 1952 No. 388 B

Analogies Between the Diffraction of Light and Electron Diffraction by Gas Molecules

By L. BRU, M. P. RODRIGUEZ and R. VEGA

Laboratorio de Fisica Alonso de Santa Cruz, Universidad de Sevilla

Communicated by G. I. Finch; *MS. received 24th September* 1951

ABSTRACT. Monochromatic light has been diffracted by a unit formed by an ensemble of slits with a common axis, in which all periodicities which a molecule can exhibit are represented. By a suitable choice of the slit areas we can, moreover, take account of the contribution to the expression of the intensity of each of these periodicities. Analysis leads to expressions similar to those used in the interpretation of the pattern obtained in electron diffraction by gases. These have been applied to the cases of benzene and carbon tetrachloride. The positions of the diffraction maxima and minima agree to within little more than one per cent with those of the corresponding electron diffraction patterns. Values found for interatomic distances (starting from the relative formula of radial distribution) also agree with the real ones within the foregoing limit.

§ 1. INTRODUCTION

The growing complexity of gaseous molecules, the structure of which it is desired to determine by means of the diffraction of electrons, has made it necessary to introduce auxiliary methods for reducing the computational work. In this connection we can cite the Sherman table method and that of punched cards (Shaffer, Shoemaker and Pauling 1946), both of which originate from the procedure used in crystallography to determine crystalline structures by means of x-rays. So far, however, no method based on an optical analogy such as the 'fly's-eye' method has been used in the case of electron diffraction (de Vos 1948).

In the determination of molecular structures by means of the diffraction of electrons, two complementary methods are actually in use; they are the so-called correlation or trial and error method and the 'radial distribution' method (Wierl 1931, Pauling and Brockway 1935). On following these procedures, the difficulty arises of obtaining an accurate estimate of the intensities of the electron diffraction rings and of locating with sufficient accuracy the positions of the maxima and minima, and it is along these lines that we have mainly directed our process of analogy.

The intensity of electrons diffracted by a gas is given by:

$$I(s) = K\sum_i\sum_j \psi_i\psi_j \frac{\sin sl_{ij}}{sl_{ij}}, \qquad \ldots\ldots(1)$$

where K is a constant, l_{ij} the distance between the atoms i and j, ψ the scattering factor of the atom and

$$s = \frac{4\pi \sin \frac{1}{2}\theta}{\lambda}, \qquad \ldots\ldots(2)$$

where θ is the angle of diffusion and λ the electron wavelength. Given the intensities and the positions of the diffraction rings, the radial distribution method leads to the values of l_{ij} and gives the following equation for the well-known radial function $D(l)$:

$$D(l) = K' \sum_1^n I_k \frac{\sin s_k l}{s_k l}, \qquad \ldots\ldots(3)$$

where K' is a constant, k refers to the order of the maximum observed and I_k is the intensity of the diffraction. Owing to the difficulty of adequately estimating the intensities, which has to be done visually, some modifications of formula (3) have been suggested, but none of them are essential (see, however, Allen and Sutton 1951). Thus, the equations to be applied in studying the molecular structures by electron diffraction are of the type:

$$\sum_i G_i \frac{\sin l_{is}}{l_{is}}, \qquad \ldots\ldots(4)$$

in which G_i are constant coefficients containing either the greater or the lesser totals.

§ 2. THE OPTICAL ANALOGY

It is evident that, in order to obtain an analogy between the diffraction of electrons by gases and the diffraction of light, we must select a diffraction grating containing intrinsically the same periodicities as the gaseous molecule and reproducing the frequency with which these periodicities occur in the molecule. For example, in the case of the molecule of benzene, which we shall study later, there are three periodicities *C–C*. Two of them are repeated six times in each case, and the other periodicity only comes in three times. The relative *C–C* distances are in the ratio $1 : \sqrt{3} : 2$.

The above conditions are fulfilled if one takes three slits with widths proportional to these last three numbers, and with areas in the ratio 6 : 6 : 3. Thus, we see that, having chosen such gratings, the amplitude of the monochromatic light diffracted is given by (1) when the diffraction pattern is observed along a certain line OY.

Consider a slit so placed as to produce a Fraunhofer spectrum. Let OZ be the optical axis of the condenser system, the slit being in the plane XY. Let $(\alpha_1, \beta_1, \gamma_1)$ and $(\alpha_2, \beta_2, \gamma_2)$ be the cosines corresponding to the directions of the incident parallel rays and of the diffracted rays respectively. These constitute a plane wave front. Supposing the optical system to be completely anastigmatic, the rays will reunite at a certain point of the focal plane of the optical system. As is known, the diffracted amplitude is represented by

$$A = r(x_2 - x_1)(y_2 - y_1) \frac{\sin \delta}{\delta} \frac{\sin \epsilon}{\epsilon},$$

$(x_2 - x_1)$ and $(y_2 - y_1)$ being the relative transverse and longitudinal dimensions of the grating, $\delta = \pi(\beta_2 - \beta_1)(y_2 - y_1)/\lambda$ and $\epsilon = \pi(\alpha_2 - \alpha_1)(x_2 - x_1)/\lambda$. The amplitude is therefore proportional to the area of the slit and independent of the position of the slit with respect to the optical axis of the system.

Supposing the unit to be made up of a series of slits with a common axis, and areas $a_1, a_2, \ldots$ each will produce a displacement e_i with angles $\delta_1, \delta_2, \delta_3, \ldots$ $\epsilon_1, \epsilon_2, \epsilon_3, \ldots$

The total amplitude will therefore be equal to

$$A = r\sum_{1}^{n}\left[a_i \frac{\sin \delta_i}{\delta_i}\frac{\sin \epsilon_i}{\epsilon_i}\right], \qquad \ldots\ldots(5)$$

where $\delta_i = \pi(\beta_2 - \beta_1)l_i/\lambda$ and $\epsilon_i = \pi(\alpha_2 - \alpha_1)n_i/\lambda$ and l_i and n_i are the width and length of the slit *i*. If the resultant wave plane advances normally to the plane of the slit we have $\alpha_1 = \beta_1 = 0$. If, in addition, we wish to study the distribution of the intensities only in a straight line parallel to the axis OY, which belongs to the focal plane of the system, we shall merely have to select those wave planes diffracted parallel to OX as they are the only ones focused in the said straight line; hence $\alpha_2 = 0$. We then have the following conditions: $\delta_i = \pi\beta_2 l_i/\lambda$, $\epsilon_i = 0$, $(\sin \epsilon_i)/\epsilon_i \to 1$.

The equation for the amplitude is then

$$A = r\left[\Sigma a_i \frac{\sin \pi\beta_2 l_i/\lambda}{\pi\beta_2 l_i/\lambda}\right].$$

The diffracted intensity is thus given by:

$$I = A^2 = r^2[\Sigma a_i (\sin sl_i)/sl_i]^2, \qquad \ldots\ldots(6)$$

with $s = \pi\beta_2/\lambda$. It is thus possible to study the maxima and minima with respect to β_2 which is the only variable.

Equation (6) is of the same form as those used in the evaluation of the gas electron-diffraction pattern. The scattering factors are here proportional to the areas a_i, and the structure of the molecule remains fixed by the parameters l_i.

Since the intensity is represented by the square of the amplitude, doubt may arise as to whether the diffraction spots observed correspond to the maxima or the minima. However, the difficulty can be easily overcome by adding to the grating used a further element whose function is to introduce a coherent amplitude, always positive, and without maxima or minima. In this way an upward direction is given to the curve of diffraction of the unit. At first sight it might appear to be simpler to add another slit of such dimensions that the whole diffraction pattern comes within the principal maximum produced by this new slit. However, as the curve of diffraction corresponding to this principal maximum descends very rapidly, it is preferable to select another additional element. For this purpose the most convenient device appears to be a wedge, the dimensions of which fit those of the original unit. As we shall see later, eqn. (6) is practically unaltered when the unit diffraction constitution is repeated *n* times, and we can derive the equation for the amplitude of the wave diffracted by a series of wedges disposed as shown in fig. 1.

If $m = a/b = d/c$, then $y = -m(x - nc)$, where n is the number of wedges. Following the general theory of the diffraction of light, we shall then have the following formula for the displacement produced by the wedge number n:

$$e_n = \int_{nc}^{nc+b} dx \int_{-m(x-nc)}^{m(x-nc)} \cos\{2\pi\alpha + (2\pi/\lambda)\sin\theta y\}\, dy,$$

which reduces to $e_n = 2ab\{(1 - \cos\mu)/\mu^2\}\cos 2\pi\alpha$, where the term $2\pi\alpha$ takes in consideration the phase, $\mu = Da$ and $D = (2\pi/\lambda)\sin\theta$.

The amplitude of diffraction in the combination of wedges is therefore equal to $A_c = 2ab\,(1-\cos\mu)/\mu^2$ which is always positive.

We have used a diffraction grating unit which consists of the appropriate representation of the molecule of known structure. For such a grating we have the following equation for the amplitude of the diffracted waves:

$$A = \Sigma A_i \frac{\sin \mu l_{ij}}{\mu l_{ij}} \frac{\sin \nu n_i}{\nu n_i} \frac{\sin \tfrac{1}{2} N \nu d}{N \sin \tfrac{1}{2} \nu d},$$

where d is the period of the grating, N the number of units and ν plays the same role as μ but in the transverse direction. The factor $\chi = (\sin \tfrac{1}{2} N\nu d)/N \sin \tfrac{1}{2}\nu d$ is that which now represents the width of the spots of diffraction. These are all equal because d and N are constants. Disturbances due to the different lengths of the slits are eliminated since the widths of the diffraction spots are uniform. We have proved by experiment the disappearance of the disturbance mentioned even when using diaphragms of relatively large diameter. The new factor is practically unity on the axis of the spot and zero outside it. Therefore in considering the diffraction in a normal direction from the axis of the slit the general equation (6) is valid.

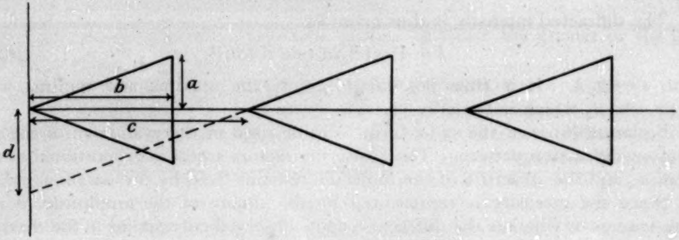

Fig. 1. Disposition of wedges.

As is natural, in utilizing the unit repeated N times, diffraction spots appear on either side of the zero order spot which, however, is the only one which needs to be taken into consideration.

§ 3. EXPERIMENTAL

To obtain the diffraction gratings two different 'fly's eyes' have been used, one containing 400 lenses and the other only 25. In obtaining the diffraction pattern only one row of units has been afterwards used on each plate exposed, the rest of the plate being covered with black cardboard.

The diffraction patterns were obtained by placing the photographic plate, on which the 'fly's eye' had been impressed, between two converging lenses with a focal distance of 2 metres. As light source a point-source mercury lamp of 250 watts was used with a series of filters giving a sufficiently monochromatic light (Bru and Cubero 1950).

In table 1 are given the distances S_{exp} separating the diffraction spots in the diagram obtained with benzene. (We have used a model, without the addition of the wedge, placed on the second fly's eye, that is to say the one which reproduces the original unit only five times.) The ratios of these distances to the corresponding theoretical values s_{th} of the diameters of the maxima and minima of the diffraction rings are given in the fourth column. As can be seen, they agree quite well. We need not be surprised at the value shown for the first maximum, as this always appears confused.

Table 1

Rings	s_{exp}	s_{th} (max)	s_{th} (min)	$s_{\mathrm{exp}}/s_{\mathrm{th}}$
I	9·0	4·1		2·20
II	11·8		5·8	2·04
III	16·2	8·1		2·00
IV	22·0		10·6	2·08
V	27·6	13·7		2·01
VI	30·0		14·7	2·04
VII	32·4	15·5		2·08
VIII	36·0		17·5	2·05

In fig. 2 (Plate) is reproduced a diagram obtained by rotating the original plate during the printing of a diapositive. In it the relative intensities are not retained but the positions of the maxima and minima are still well shown. Both are represented by white rings, maxima and minima alternately.

In order to see the effect of the wedge, plates were exposed with the first 'fly's eye', one with the unit alone and the other with the unit and the wedge. Thus we get a series of units of slits (fig. 3 (*a*), Plate) and a series of units formed by slits and wedges (fig. 3 (*b*), Plate). The dimensions of the combinations were:

	1st slit	2nd slit	3rd slit	Wedge
Width (mm)	200	172	100	24
Length (mm)	12	25	45	160

In fig. 4 the theoretical form of the diffraction curves of the model, of the wedge, and the sum of both are reproduced.

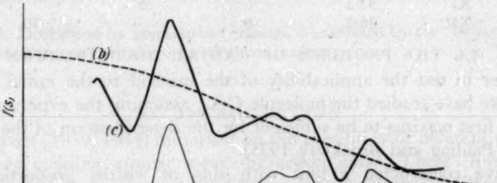

Fig. 4. Influence of the wedge in the diffraction curves of the benzene model formed with slits only. (*a*) Theoretical curve of model, (*b*) curve of wedge, (*c*) sum of model and wedge.

The interpretation of both plates is given in tables 2 and 3, together with the intensities of the diffraction spots obtained.

As can be seen, only four spots appear, corresponding to the four first maxima of diffraction. The second minimum intensity has disappeared and the fourth maximum has made its appearance. In fig. 5 (Plate) both diagrams are reproduced. It will be seen that the employment of the wedge has avoided any possible ambiguity in the identification of the maxima.

Table 2

Rings		s_{exp}	Theoretical Max.	Theoretical Min.	$s_{\text{exp}}/s_{\text{th}}$
I	vs	6·2	1		1·50
II	vs	10·2		2	1·88
III	vs	15·0	2		1·86
IV	s	19·6		3	1·90
V	w	25·6	3		1·90

Table 3

I	s	8·0	1	1·97
II	vs	15·4	2	1·90
III	w	25·0	3	1·92
IV	w	29·5	4	1·90

Carbon tetrachloride. In table 4 we reproduce the data corresponding to fig. 6 (Plate) obtained without using the wedge, as this was not necessary for the identification of the maxima and minima. It will be seen that the agreement is excellent.

Table 4

Rings	s_{exp}	Max.	Min.	$s_{\text{exp}}/s_{\text{th}}$
I	4·9		1	
II	7·3	1		2·51
III	10·0		2	
IV	13·2	2		2·72
V	16·4		3	
VI	19·8	3		2·75
VII	22·4		4	
VIII	25·0	4		2·71
IX	27·7		5	
X	30·8	5		2·71
XI	33·1		6	
XII	36·2	6		2·70

§ 4. THE PROBLEM OF RADIAL DISTRIBUTION

In order to test the applicability of the method to the radial distribution problem, we have studied the molecule CCl_4, assuming the experimental values of the five first maxima to be sufficient for the determination of the interatomic distances (Pauling and Brockway 1935).

We have constructed a unit with slits of widths proportional to the experimental s_k and with areas proportional to the visual I_k (fig. 7, Plate). The diffraction amplitude across this unit will be found to be given by the formula

$$A = r\Sigma A_k \frac{\sin a_k(\pi/\lambda)\sin\theta}{a_k(\pi/\lambda)\sin\theta},$$

and, taking into account the large focal distances of our lenses, we have $\sin\theta = \theta = l/L$ whence

$$A = r\Sigma A_k \frac{\sin a_k(\pi/L\lambda)l}{a_k(\pi/L\lambda)\,l}.$$

Comparing this formula with (3) we have $l = d\dfrac{a_k}{s_k}\dfrac{\pi}{L\lambda}$.

In the apparatus used $L\lambda = 1{\cdot}13\ \text{mm}^2$. If we measure a_k and d in millimetres and s_k in Å^{-1}, l will be in units of Å.

In table 5 are given the values for CCl_4.

Table 5

k	1	2	3	4	5
I_k	20	30	10	15	5
a_k	1·1	1·9	2·7	3·5	4·3
s_k	2·93	4·91	7·13	9·23	11·34

In the diffraction pattern the distance d is 2·7 mm, from which it follows that $l = 2{\cdot}87$ Å, which agrees well with the experimental value 2·85Å obtained by the conventional methods of calculation. The diffraction pattern obtained is reproduced in fig. 8 (Plate).

REFERENCES

Allen, P. W., and Sutton, L. E., 1951, *Trans. Faraday Soc.*, **47**, 236.
Bru, L., and Cubero, M., 1950, *An. Soc. esp. Fis. Quim.* A, **46**, 317.
Crowfoot, D., and Bunn, C. W., 1949, *The Chemistry of Penicillin* (Princeton : University Press).
Pauling, L., and Brockway, L. O., 1935, *J. Amer. Chem. Soc.*, **57**, 2648.
Shaffer, P. A., Shoemaker, V., and Pauling, L, 1946, *J. Chem. Phys.*, **14**, 648 and 659.
Thomson, G. P., and Cochrane, W., 1939, *Theory and Practice of Electron Diffraction* (London : Macmillan).
de Vos, P., 1948, *Acta Crystallogr.*, **1**, 247.
Wierl, R., 1931, *Ann. Phys., Lpz.*, **8**, 521.

.B
5
2

Homometric Diffraction Gratings

By L. BRU, M. CUBERO and J. GARRIDO
Laboratorio de Fisica Alonso de Santa Cruz, Universidad de Sevilla

Communicated by G. I. Finch; MS. received 24th September 1951

ABSTRACT. Diffraction by homometric gratings is examined by the 'fly's eye' device. The patterns obtained confirm the theoretical conclusions.

§ 1. INTRODUCTION

Patterson (1939, 1944) remarked on the possibility of different crystalline structures yielding similar x-ray diffraction data. These 'homometric' structures although geometrically different have the same $|F(hkl)|$ amplitudes. One of us (J. G.) has studied the problem of homometric structures from the point of view of the uniqueness or otherwise of the analytical results of the corresponding x-ray diffraction, and has been able to determine the conditions necessary for the existence of such structures. We thought that it would be interesting to examine optically these conclusions and to study the diffraction of the light by means of two-dimensional gratings which, although geometrically different, produce the same Fraunhofer spectrum.

§ 2. CONSTRUCTION OF THE HOMOMETRIC GRATINGS

The gratings used have been constructed with the help of the 'fly's eye' method of Stokes (1946) by multiple photography of a unit consisting of circles and rings representing the atoms of the elementary parallelogram. The diameter of the filled-in circles was 4 cm and the diameters of the rings which represent atoms of atom factor smaller than those represented by filled-in circles were calculated according to the method of de Vos (1948). The 400 units combined in the photograph were 1 millimetre apart.

The units employed to construct the homometric gratings were some of those described in the above mentioned study of the uniqueness of the structures, the object being reduced to two dimensions. We will omit the theoretical considerations as these have already been fully discussed by Garrido (1952). Diffraction was effected with an ordinary mounting fitted with two lenses at a focal distance of 2 metres, and a point-source mercury lamp of 250 watts, fitted with appropriate filters.

§ 3. RESULTS

Experiments were carried out with each of the three types of homometric gratings, that is to say (i) gratings formed by 'identical atoms' distributed in different ways, (ii) gratings formed by the same numbers of different 'atoms' distributed in different ways, and (iii) gratings formed by different numbers of different 'atoms'.

An example of type (i) is to be found in the two gratings of the photograph (Plate), each of which contains four 'atoms' identical in the elementary parallelogram, but differently disposed in each grating. Calculations show that the diffraction amplitudes should be similar in both cases, although the phases are different. Within the limits of experimental error the results confirm theoretical conclusions.

REFERENCES

Garrido, J., 1952, *Bull. Soc. F. Min. Crist.*, in the press.
Patterson, A. L., 1939, *Nature, Lond.*, **143**, 939; 1944, *Phys. Rev.*, **63**, 195.
Stokes, A. R., 1946, *Proc. Phys. Soc.*, **58**, 306.
de Vos, P., 1948, *Acta Crystallogr.*, **1**, 246.

The Virtual Optics of the Median Plane of Axially Symmetric Magnetic Prisms*

By J. C. E. JENNINGS
Birkbeck College, Malet Street, London W.C.1

Communicated by W. Ehrenberg; *MS. received* 8th *October* 1951

ABSTRACT. The angle between the asymptotes of a ray is developed as a power series in its impact parameter about some value which characterizes the 'principal ray'. When this value is zero, the principal points of the equivalent lens coincide at the axis of symmetry; in all other cases it is 'thick'. The focal length is here associated with the coefficient of the linear term, the transverse aberrations with those of the higher terms. The quadratic aberration vanishes for a wide range of relative $H\rho$ if the principal ray is suitably chosen. Foci with quadratic aberration are intercepts of the caustic curve, whose cusp lies at the cubic focus. The dependence of aberration upon magnification and the conditions in which the cubic as well as the quadratic aberration vanish are discussed.

---

* This paper includes material from Part II of a Thesis (1950) approved by the University of London for the degree of Ph.D.

§ 1. INTRODUCTION

Herzog (1934) pointed out that discontinuous sector fields, normal to the plane of motion of the electrons considered, combine the properties of a prism and of a cylindrical lens; this applies equally to continuous fields and must be understood when they are described, following Siday (1947), as magnetic prisms. Since the analogues of spherical lenses are also widely used in electron spectroscopy, Siday's nomenclature is obviously preferable to that of Smythe, Rumbaugh and West (1934) and Kerwin (1950) who call sector fields 'magnetic lenses'.

The current terminology regarding orders of aberration is also unsatisfactory. When the lowest order transverse (or angular) aberration depends on the second, third or fourth power of the aperture, we shall speak of quadratic, cubic or quartic aberration and shall call the condition quadratic, cubic or quartic focusing. 'Second order focusing' has been used by Stephens (1934), Kerwin (1949, 1950) to mean quadratic focusing, but by Bock (1933), Hintenberger (1948 a, 1949) and Judd (1950) to mean cubic focusing.

There have been many proposals for the suppression of quadratic aberration, or even of all aberration, in magnetic prisms (Korsunsky 1944, 1945, Bainbridge 1947, Hintenberger 1948 a, b, 1949, Kerwin 1949, 1950, Kerwin and Geoffrion 1949, Spighel 1949). All, however, refer to discontinuous fields and the cautious view of Judd (1950) that "second order effects .... are thought to be of the same order as corrections for the fringing field" is doubtless justified. Some authors have used the theory of Coggeshall (1947) to estimate the paraxial effects of the fringing field, but before Ploch and Walcher (1950) there had been no attempt to estimate the effect of the fringing field upon the aberration; and the integrals which the latter give are valid only for a 'thin' fringing field, i.e. for a case in which the trajectories in the uniform field and in zero field are long compared with those in the fringing field. But comparison between, on the one hand, measurements (Ehrenberg and Jennings 1952, to be referred to as EJ) and calculations (Jennings 1950, § IV, 6) for separated poles and, on the other hand, the limiting case of Korsunsky's prism (Jennings 1950, § IV, 2) shows that aberration-dependent properties of continuous fields cannot be inferred from the limiting discontinuous case.

The fields whose optical properties are studied in this paper are axially symmetric and everywhere normal to the plane to which the rays considered are confined. This plane is conveniently called the 'median plane', for it will usually be the median plane between two equal and opposite poles. In it the field is a function only of the radial coordinate, so that the trajectories may be solved in terms of an integral (Coggeshall and Muskat 1944). If the fields are subject to the further restriction that $n > 2$, where $\lim_{r \to \infty} H(r) \propto r^{-n}$, then asymptotes to the trajectories exist (Coggeshall and Muskat 1944). As was first pointed out by Siday (1947), a great simplification results if these asymptotes, which, following him, we shall call virtual rays, are considered instead of the real rays (i.e. the trajectories). For virtual rays and axial symmetry, the dependence of aberration upon magnification, together with other useful relations, may be simply developed; this is the subject of the present paper.

The field due to a pair of uniform circular plane poles is of especial interest. In the first place, in the limiting case of zero pole separation (Korsunsky 1944, 1945), the prism is aplanatic for infinity and the focal point, for one value of the relative electron momentum; thus this class of prism is, prima facie, certainly not inferior to any of the geometrically more complicated sector fields which have been proposed. In the second place (Jennings 1950, Appendices 1 to 3) the magnetic field and vector potential can be expressed in terms of tabulated functions and hence the optical properties can be calculated. Siday (1947) calculated some of the properties of such a prism for a pole separation of one radius and gave an expression for the dependence upon magnification. The experiments reported in II were based on his theory and led to the development of the more general analytical theory which is the subject of the present paper.

§ 2. ANGULAR ABERRATION

With Siday we denote a ray, for any given ratio $H_0/H\rho \equiv \Psi$ (where H_0 is the field strength on the axis in the median plane), by its 'impact parameter' b, which is the perpendicular distance of its asymptotes from the axis; evidently from the axial symmetry of the field b is the same for the incident and refracted asymptotes of any one ray. The parameter b is thus zero for virtual rays which pass through the axis of symmetry and it is taken as positive for those which pass through less of the field, i.e. which are less deflected, than the ray $b=0$.

In the figure the point X is a virtual source of monochromatic electrons; rays of parameters 0, b_1, b_2 and b are shown, which suffer deflections $\pi-2\theta_0$, $\pi-2\theta_1$, $\pi-2\theta_2$ and $\pi-2\theta$ respectively. Consider the conditions under which rays with parameters near to b_1 may be focused. For this purpose, let $x=b-b_1$.

For monochromatic rays in a given field, the angle θ defined above is evidently a function only of b (or x). It may therefore be expanded:

$$\theta=\theta_1+\lambda x+\mu x^2+\nu x^3+\sigma x^4+\tau x^5+\ \dots \qquad \dots\dots(1)$$

where θ_1, λ, μ, etc. are functions of b_1 as well as of Ψ.

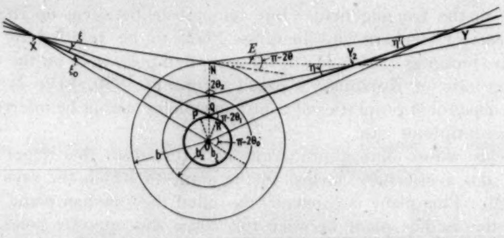

Virtual imagery by a thick prism. X is an object point. The principal incident and refracted rays and the circle b_1 are drawn in bold lines. All angles shown are positive.

Let the ray b_2 be paraxial with respect to the ray b_1; then Y_2 is the paraxial image of X and YY_2 is the longitudinal aberration of the marginal ray b. OR is perpendicular to RX, OP to PY. As will be shown, R and P are the object and image principal points respectively and distances will be measured along the principal ray b_1, so that $RX=u$, $PY_2=v$. NY_2 is a tangent to the circle of radius b. Q is the intersection of ON with PY. The angle $\eta=N\hat{Y}_2P$. The angle between the incident rays b and b_1 is ξ, that between the refracted rays is η'. The angular aberration of the marginal ray b is $E=\eta-\eta'$.

When $b>b_1$, η and η' are each greater than zero. If the marginal ray is underfocused (as in the figure), then $\eta>\eta'$ so that $E>0$. For a marginal ray

$b_3 < b_1$ which is also underfocused to Y, $E < 0$. Thus on this convention there is marginal underfocusing if E is always of the same sign as x as, for example, if $k > 0$ where $E = kx^3$. This sign convention for k is opposite to that used in lens optics; its convenience is that it gives a positive sign to the cubic aberration so far always found in axially symmetric prisms.

From the figure $\xi + \eta' = 2(\theta - \theta_1)$ so that

$$E = \eta + \xi - 2(\theta - \theta_1). \qquad \ldots\ldots(2)$$

Now, $$\sin \eta = \frac{\mathrm{NQ}}{\mathrm{Y_2Q}} = \frac{\mathrm{NO} - \mathrm{OQ}}{\mathrm{Y_2P} - \mathrm{PQ}} = \frac{b - b_1 \sec \eta}{v - b_1 \tan \eta}.$$

Similarly $$\sin \xi = \frac{b - b_1 \sec \xi}{u - b_1 \tan \xi} \qquad \ldots\ldots(3)$$

whence $$\sin \xi = \frac{bu - [b^2u^2 - (b^2 - b_1^2)(u^2 + b_1^2)]^{1/2}}{u^2 + b_1^2}$$

wherein only the negative sign is needed before the surd since $\sin \xi = 0$ when $b = b_1$. Substitution of $b = x + b_1$ gives

$$(u^2 + b_1^2) \sin \xi = u(b_1 + x) - b_1 u[1 - (x/u^2)(2b_1 + x)]^{1/2}.$$

If $x/u \ll 1$ and $2b_1/u$ is not very much greater than 1, the surd may be expanded by the binomial theorem. Neglecting terms higher than x^3 we have

$$\sin \xi = \frac{x}{u} + x^2 \frac{b_1}{2u^3} + x^3 \frac{b_1^2}{2u^5}.$$

(The coefficient of x^4 in this series is much more complicated than those of lower powers.) To the cubic approximation

$$\xi = \frac{x}{u} + x^2 \frac{b_1}{2u^3} + x^3 \left(\frac{b_1^2}{2u^5} + \frac{1}{6u^3}\right) \qquad \ldots\ldots(4)$$

$$\eta = \frac{x}{v} + x^2 \frac{b_1}{2v^3} + x^3 \left(\frac{b_1^2}{2v^5} + \frac{1}{6v^3}\right). \qquad \ldots\ldots(5)$$

The inverse of eqn. (4) is found by expressing x in terms of expanded trigonometric functions of ξ from eqn. (3):

$$x = u\xi - \frac{b_1}{2}\xi^2 - \frac{u}{6}\xi^3 + \frac{b_1}{24}\xi^4 + \frac{u}{120}\xi^5 \ldots \qquad \ldots\ldots(6)$$

Substitution in eqn. (2) from eqns. (1), (4) and (5) gives:

$$E = x\left[\frac{1}{u} + \frac{1}{v} - 2\lambda\right] + x^2\left[\frac{b_1}{2}\left(\frac{1}{u^3} + \frac{1}{v^3}\right) - 2\mu\right]$$
$$+ x^3\left[\frac{1}{6}\left(\frac{1}{u^3} + \frac{1}{v^3}\right) + \frac{b_1^2}{2}\left(\frac{1}{u^5} + \frac{1}{v^5}\right) - 2\nu\right]. \qquad \ldots\ldots(7)$$

Now, the angular aperture at the object is ξ, which, to the paraxial approximation, is x/u (from eqn. (4)). Hence eqn. (7) shows that the angular aberration E contains no term linear in aperture, provided that $1/u + 1/v = 2\lambda = 1/f$, say, where λ is a constant with respect to variation of u and v. This result proves that R and P in the figure are the principal points and that the criterion of focusing with respect to a given principal ray is that the linear term in the angular aberration should vanish, where, of course, the angular aperture is measured from that principal ray.

Provided that v, the distance of the receiving screen from the image principal point, is chosen to satisfy $1/u+1/v=1/f$, then eqn. (7) reduces to:

$$E=x^2\left[\frac{b_1}{2}\left(\frac{1}{u^3}+\frac{1}{v^3}\right)-2\mu\right]+x^3\left[\frac{1}{6}\left(\frac{1}{u^3}+\frac{1}{v^3}\right)+\frac{b_1^2}{2}\left(\frac{1}{u^5}+\frac{1}{v^5}\right)-2\nu\right]\quad\ldots\ldots(8)$$

If $u=\infty$, let $E=e$, where

$$e=x^2\left[\frac{b_1}{2f^3}-2\mu\right]+C\left(\frac{x}{f}\right)^3\qquad\ldots\ldots(9)$$

where

$$C=\tfrac{1}{6}+b_1^2/2f^2-2\nu f^3.\qquad\ldots\ldots(10)$$

If $u=v=2f$, let $E=E_1$, where

$$E_1=x^2\left[\frac{b_1}{8f^3}-2\mu\right]+x^3\left[\frac{1}{24f^3}+\frac{b_1^2}{32f^5}-2\nu\right].\qquad\ldots\ldots(11)$$

When $b_1\neq 0$ the lateral magnification is no longer given by $m=v/u$. From the axial symmetry of the field it is obvious that an object, forming an arc of a circle centred on the axis of symmetry, must be imaged as an arc of a concentric circle, subtending the same angle at the centre. Therefore

$$m^2=(v^2+b_1^2)/(u^2+b_1^2).\qquad\ldots\ldots(12)$$

With the help of eqn. (6) it is simple, although cumbersome, to express eqn. (8) for E in terms of ξ, but this is not necessary for determining the conditions under which the coefficients of successively higher powers of ξ vanish. Such conditions are sought, for any given power, under the assumption that they already hold for all lower powers; thus, for example, there is no point in suppressing quadratic aberration without at the same time focusing the image. None the less, if the intensity distribution at the image of an extended object is to be calculated, it may be necessary to know the aberration coefficients at places other than the paraxial focus; but for this purpose the transverse, not the angular, aberration is required.

§ 3. TRANSVERSE ABERRATION

The transverse aberration S observed on a screen perpendicular to the principal ray b_1 may be derived in a way similar to that for E, giving

$$S=(x+b_1)\sec\eta'-b_1-v\tan\eta'.\qquad\ldots\ldots(13)$$

The functions $\sec\eta'$ and $\tan\eta'$ may be expanded as power series in $\eta'=2(\theta-\theta_1)-\xi$. Equation (1) expresses $\theta-\theta_1$ in terms of x, so that S is known in terms of x and ξ. With the help of eqn. (4) or (6) it may therefore be obtained as a power series in either x or ξ alone. For calculating the intensity distribution in the image, it is generally desirable to express S in terms of ξ; but if $u\to\infty$, then $\xi\to 0$, and $u\xi\to x$ where x is the effective aperture. To the cubic approximation

$$S=\xi(u+v-uv/f)+\xi^2(\tfrac{1}{2}b_1\alpha^2-\tfrac{1}{2}b_1-\beta v)+\xi^3(\tfrac{1}{2}\alpha^2u+b_1\alpha\beta-\tfrac{1}{6}u-\gamma v-\tfrac{1}{3}\alpha^3v)\quad.(14)$$

where

$$\alpha=u/f-1,\ \beta=2\mu u^2-b_1/2f,\ \gamma=2\nu u^3-2\mu b_1u-u/6f.$$

If, as in the experiments described in EJ, $u\to\infty$, S is obtained in terms of x alone and it is then simple and useful to obtain the quartic approximation. At the focal point

$$S=x^2[b_1/2f^2-2\mu f]+x^3[1/6f^2+2b_1\mu/f-2\nu f]+x^4[2b_1\mu^2+2b_1\nu/f+5b_1/24f^4-2\sigma f].\quad\ldots\ldots(15)$$

As one would expect, the quadratic term is equal to f times the quadratic term in e (eqn. (9)), but this relation does not hold between the cubic terms, viz.,

from S: $1/6f^2-2\nu f+2b_1\mu/f$
from ef: $1/6f^2-2\nu f+b_1^2/2f^4$.

These agree only if $2b_1\mu/f=b_1^2/2f^4$, that is, if $b_1=0$ or if $\mu=b_1/4f^3$. The former is the 'thin prism' condition, the latter is that for no quadratic aberration. It seems likely that in general for a thick prism the nth order term in S is f times that in e, if and only if all terms of lower order are zero.

If the perpendicular to the screen is inclined at an angle δ to the ray b_1, the transverse aberration observed on it will be

$$S_\delta=\frac{S\cos\eta'}{\cos(\delta+\eta')}=\frac{S\sec\delta}{1-\tan\delta\tan\eta'}=S\sec\delta(1+\tan\delta\tan\eta'+\tan^2\delta\tan^2\eta'+\dots) \qquad \dots\dots(16)$$

provided that $\tan\delta\tan\eta'<1$. A power series in x can be formed for $\tan\eta'$, the first term of which is x/v. Hence

$$S_\delta=S\sec\delta[1+(x/v)\tan\delta\ \dots\ .]. \qquad \dots\dots(17)$$

§ 4. CUBIC FOCUSING BY A THIN PRISM

From the figure it is clear that when $b_1=0$ the principal points R and P coincide at O, that is, the prism is then in this sense 'thin'.

Siday confined attention to the thin prism, inasmuch as he regarded the ray $b=0$ as the principal ray. Without expressing θ as a power series, as in eqn. (1), he found

$$e-E=b^3/2f_0uv \qquad \dots\dots(18)$$

which agrees with eqns. (8) and (9) if b_1 is put equal to zero. Because he did not assume an analytical form for θ, and therefore for e, Siday directed attention to the total aberration, not to coefficients in its development. He computed e for various values of Υ, for a uniform pole prism having a pole separation of one radius. He found that, at one value of Υ, e was approximately antisymmetric about $b=0$ and then varied as $|b^3|$. At other values of Υ, e neither was antisymmetric nor obeyed a cubic law on either side of $b=0$. The coincidence of antisymmetry and a cubic law is not fortuitous, for eqn. (9) shows that e is the sum of quadratic, cubic and higher terms. Inevitably, therefore, antisymmetry and a cubic law go together if quintic and higher terms are negligible. If for the case $b_1=0$ eqn. (1) is re-written in the form:

$$\theta=\theta_0+\lambda_0 b+\mu_0 b^2+\nu_0 b^3+\sigma_0 b^4+\tau_0 b^5+\ \dots\dots \qquad \dots\dots(19)$$

then the condition which Siday found was that $\mu_0=0$; θ_0, $\lambda_0(\equiv 1/2f_0)$, μ_0, etc. are functions of Υ.

§ 5. CUBIC FOCUSING BY A THICK PRISM

The experiments reported in II show that e is cubic over a wide range of Υ, a result which at first sight appears to be inconsistent with Siday's calculations. It was this observation that led to the development of the thick prism theory, that is, to the consideration of $b_1\neq 0$. Apart from the development of θ (eqn. (1)) and hence of E (eqn. (8)) as a series, the basis of the theory is the well-known fact that any cubic expression x^3+ax^2+bx+c can be transformed to $x_1^3+a_1x_1+b_1$ by the linear transformation $x=x_1-a/3$.

The quadratic term in eqn. (9) vanishes if

$$\mu=2b_1\lambda^3. \qquad \dots\dots(20)$$

It will be convenient to denote by b_{13} a value of b_1 about which there is no quadratic aberration at the magnification considered, and to write $f_3=f(b_{13})$, $\lambda_3=1/2f_3$, $\mu_3=\mu(b_{13})$, etc. For the particular case of $u=\infty$, the cubic aberration coefficient is C, defined in eqn. (10). This will be specially denoted as follows: if

$$b_1=0,\ C=C_0;\ b_1=b_{13},\ C=C_3;\ b_{13}=0,\ C=C_{03}. \qquad \ldots\ldots(21)$$

In the experiments reported in EJ, b_1 could always be so chosen that the real focusing was cubic. In order to calculate whether the virtual focusing can be made cubic, it is necessary to know λ (and thence μ) as a numerical function of b_1 or to be able to express λ and μ as power series in b_1. The second method gives simple solutions for b_{13} only in the neighbourhood of the value of b_1 about which the expansion is made. As an illustration, let the expansion be about $b_1=0$. From the simultaneous validity of eqns. (1) and (19) it follows that

$$\lambda=\lambda_0+2\mu_0 b_1+3\nu_0 b_1^2+4\sigma_0 b_1^3+5\tau_0 b_1^4+\ \ldots . \qquad \ldots\ldots(22)$$

$$\mu=\mu_0+3\nu_0 b_1+6\sigma_0 b_1^2+10\tau_0 b_1^3+\ \ldots . \qquad \ldots\ldots(23)$$

$$\nu=\nu_0+4\sigma_0 b_1+10\tau_0 b_1^2+\ \ldots . \qquad \ldots\ldots(24)$$

Equations such as (22–24) are of great importance, for they make it possible to calculate optical properties about one principal ray when the available data refer to another.

If b_{13} is small enough, λ_3 and μ_3 are given by eqns. (22) and (23). To the first approximation, therefore, eqn. (20) becomes $\mu_0+3\nu_0 b_{13}=2\lambda_0^3 b_{13}$ or

$$b_{13}\simeq\mu_0/(2\lambda_0^3-3\nu_0). \qquad \ldots\ldots(25)$$

Evidently from eqns. (10) and (21)

$$3C_0/2f_0^3=2\lambda_0^3-3\nu_0. \qquad \ldots\ldots(26)$$

Combining eqns. (25) and (26), we have

$$b_{13}\simeq 2\mu_0 f_0^3/3C_0. \qquad \ldots\ldots(27)$$

Experiment and computation show that, when b_{13} is small, f_0 is of the order of the pole radius, except that at great pole separations it is probably of the order of the pole separation. Thus, if, at a particular value of Ψ, $\mu_0=0$ and $C_0\neq 0$, at a neighbouring value of Ψ, b_{13} will be given by eqn. (27); that is, cubic focusing, if it occurs at all, occurs over a range of Ψ in any axially symmetric prism (assuming f_0, μ_0 and C_0 to be well-behaved functions of Ψ). Equation (27) also shows that the smaller C_0 is, the more rapidly does b_{13} change with μ_0 and therefore with Ψ. That this holds for real imagery is borne out by the experimental curves (EJ, fig. 8) of b_{13}/a against $a\Psi$ (where a is the pole radius) for various pole separations; the steepest slope is that for the closest pole separation. Equation (27) does not apply at zero pole separation and $a\Psi=1$ (Korsunsky's case); if the limit of b_{13} is taken as $a\Psi\to 1$ it is found that $b_{13}\to -a$, which is outside the range of validity of eqn. (27).

§ 6. QUARTIC FOCUSING

Whilst it appears that at any pole separation an axially symmetric prism exhibits cubic focusing at all magnifications and over a wide range of Ψ, there may also be quartic focusing (i.e. suppression of all terms in eqn. (8) below the fourth order) at certain pole separations and magnifications; but it cannot be expected to occur for a range of Ψ.

As Siday pointed out, in the thin prism the maximum of $e-E$ (eqn. (18)) is $e-E_1=b^3/8f_0{}^3$. Hence there will be quartic focusing at unit magnification at that value of Ψ at which $\mu_0=0$, provided that $C_{03}=0{\cdot}125$. There can never be quartic focusing by a thin prism of which $C_{03}>0{\cdot}125$. If $C_{03}<0{\cdot}125$, quartic focusing will occur at some value of u between ∞ and $2f_0$ and, from the symmetry of the prism, also at the conjugate value between $2f_0$ and f_0. Experiment and computation show that at a pole separation of one radius, C_{03} is about 0·2 to 0·3; at zero pole separation, which is Korsunsky's case, $C_{03}=0$. Quartic focusing is therefore possible with thin prisms having a pole separation not exceeding about one half of the pole radius.

The theory of the thick prism shows extended possibilities of quartic focusing. Thus, at unit magnification (see eqn. (11)) the required conditions are $b_1\nu=\mu(\frac{1}{3}+\lambda^2b_1{}^2)$ and $b_1\lambda^3=2\mu$.

Using eqns. (22–24) for small b_1, and neglecting $b_1{}^2$ and higher powers we obtain $\lambda_0{}^3=6\nu_0$ and $\mu_0=0$, which correspond to $b_1=0$, the thin prism.

Taking $b_1{}^2$ into account, we get the first thick prism approximation:

$$b_1{}^{-2}=3(2\sigma_0/\mu_0-\lambda_0{}^2) \qquad \ldots\ldots(28)$$

and

$$4\mu_0=(\lambda_0{}^3-6\nu_0)[3(2\sigma_0/\mu_0-\lambda_0{}^2)]^{-1/2}. \qquad \ldots\ldots(29)$$

From eqn. (29) it appears most unlikely that quartic focusing should occur over a range of values of Ψ. Also it appears that at a quartic focus b_{13} changes very rapidly with Ψ. Consider as an example the case when b_{13} is small and $u=v$. From eqn. (11), $b_{13}\lambda^3=2\mu$. But if b_{13} is small, λ and μ may be expressed in terms of λ_0, μ_0, ν_0 from eqns. (22) and (23). To a first approximation, $b_{13}=2\mu_0/(\lambda_0{}^3-6\nu_0)$. This may be compared with eqn. (25), which refers to $u=\infty$. As in that case, so here b_{13} must vary rapidly with μ_0 and therefore with Ψ if the denominator is small. Equation (11) shows that at a quartic focus $\lambda_0{}^3=6\nu_0$ for unit magnification and a thin prism.

§7. DISPERSION AND THE CAUSTIC CURVE

Provided that the ultra-focal field (i.e. that beyond object and image) is weak, it is reasonable to suppose (cf. Siday 1947, §6) that real and virtual focusing properties will be similar and hence, in particular, that there will be real cubic focusing over a range of Ψ; this has been confirmed experimentally (see EJ). As Siday pointed out, either the real or the virtual properties of a prism may be practically important, depending on the experimental arrangement; thus, while this section explicitly refers to real focusing, it may be applied, *mutatis mutandis*, to the virtual case.

Since there is cubic focusing over a range of Ψ, the rational way of setting a photographic plate to receive a spectrum is tangentially to the locus of cubic foci. If s is arc length along this locus, the corresponding definition of dispersion is $D=\Psi ds/d\Psi$.

If the image position is described by Cartesian coordinates x, y whose origin is the centre of symmetry of the field, the positive direction of x being that of the incident ray $b=0$, then

$$x=v\cos(\omega+\xi_0)-b_1\sin(\omega+\xi_0),\ y=v\sin(\omega+\xi_0)+b_1\cos(\omega+\xi_0) \qquad \ldots\ldots(30)$$

where ξ_0 (see figure) is the angle between the incident rays 0 and b_1, and where the deflection suffered by the ray b_1 is $\omega=\pi-2\theta_1$. Evidently $ds/d\Psi$ can be calculated from $dx/d\Psi$ and $dy/d\Psi$, and the slope of the locus of foci will be given by $dy/dx=(dy/d\Psi)(d\Psi/dx)$. This shows that both slope and dispersion will be different if b_{13}, which is a function of Ψ, is used instead of some constant value of b_1.

Certain disadvantages might appear to be associated with placing the screen along the locus of cubic foci. (i) Only one point of an extended object which is perpendicular to a radius vector will be in focus, because the locus of cubic foci is not an arc of a circle centred on the axis of symmetry; it is possible, however, so to tilt the object that its image lies along the locus of cubic foci. (ii) In so far as the locus of cubic foci is not perpendicular to the principal ray b_{13}, the cubic aberration will be increased and a contribution will also be made to the quartic aberration; this may add to or subtract from the intrinsic quartic aberration. (iii) For a range of Ψ, a range of b_{13} is needed, so that a wider aperture must be accepted from the source than would be required for one value of Ψ only. For example, more recent calculations (Jennings 1950, § IV, 6.5) for the case considered by Siday show that, with $u=\infty$, b_{13} changes (near $b_{13}=0$) by 7% of the pole radius for a change of 10% in Ψ. However, it does not appear that, with cubic aberration, the resolution is seriously impaired by increasing the aperture.

These inconveniences, in any case not serious, are outweighed by that associated with the attempt (easily conceived but not so easily realized) to use the same b_1 over a range of Ψ. For if $b_1 \neq b_{13}$ then the aberration about it will be quadratic and there will be a second quadratic focus about $b_1' \simeq 2b_{13}-b_1$. Thus there will be two neighbouring images whose appearance will be that of just resolved spectral lines. It may be shown (Jennings 1950, § II, 2.8.2) that the locus of these quadratic foci (where Ψ is kept constant) has the same equation as the caustic curve which is associated with cubic aberration, viz. $y^2=4x^3/27Cf$. This reinforces the conclusion that the cubic foci are the only rational ones to use, the quadratic foci merely being intercepts of the caustic curves.

§ 8. CONCLUSION

The theory of the thick prism has shown that an axially symmetric magnetic prism can be used as a *spectrograph*, i.e. for the simultaneous photographic recording of a range of Ψ at approximately uniform resolution, in addition to its use as a *spectrometer* operating with a Geiger counter and recording one Ψ at a time. Axially symmetric prisms share with other prisms the advantage that source and detector can be outside the field; but neither these other prisms nor the immersion systems (e.g. Korsunsky, Kelman and Petrov 1944, 1945 and Dzhelepov and Bashilov 1950, Beiduk and Konopinski 1948 and Hedgran, Siegbahn and Svartholm 1950) so far proposed appear to suppress quadratic aberration save for one value of Ψ. Axially symmetric magnetic prisms suppress it over a range of Ψ and are therefore the first improvement on the semicircular focuser as a spectrograph. Remarkable as this property is, it is perhaps even more remarkable that it is not peculiar to any one axially symmetric field. The practical importance of the generality of this property is too obvious to need further emphasis. It will, of course, be important to discover how far the axial symmetry may be reduced while retaining this property.

ACKNOWLEDGMENTS

The work described in this paper was carried out in the Research Laboratory, Birkbeck College, University of London (director, Professor J. D. Bernal).

The author acknowledges the receipt of a maintenance grant from the Ministry of Education under the Further Education and Training Scheme.

Part of the work was carried out during the tenure of a research assistantship provided by the Department of Scientific and Industrial Research under a scheme directed by Mr. R. E. Siday for the development of high-precision β-spectroscopy.

The author thanks Dr. W. Ehrenberg and Mr. R. E. Siday for many helpful and encouraging discussions.

REFERENCES

Bainbridge, K. T., 1947, *7th Solvay Congress in Chemistry*.
Beiduk, F. M., and Konopinski, E. J., 1948, *Rev. Sci. Instrum.*, **19**, 594.
Bock, C. D., 1933, *Rev. Sci. Instrum.*, **4**, 575.
Coggeshall, N. D., 1947, *J. Appl. Phys.*, **18**, 855.
Coggeshall, N. D., and Muskat, M., 1944, *Phys. Rev.*, **66**, 187.
Dzhelepov, B. S., and Bashilov, A. A., 1950, *Izv. Akad. Nauk. SSSR, Ser. Fiz.*, **14**, (3) 263.
Ehrenberg, W., and Jennings, J. C. E., 1952, *Proc. Phys. Soc.* B, **65**, 265.
Hedgran, A., Siegbahn, K., and Svartholm, N., 1950, *Proc. Phys. Soc.* A, **63**, 960.
Herzog, R., 1934, *Z. Phys.*, **89**, 447.
Hintenberger, H., 1948 a, *Z. Naturforsch.*, **3a**, 125 ; 1948 b, *Ibid.*, 669 ; 1949, *Rev. Sci. Instrum.*, **20**, 748.
Jennings, J. C. E., 1950, *Ph. D. Thesis*, University of London.
Judd, D. L., 1950, *Rev. Sci. Instrum.*, **21**, 213.
Kerwin, L., 1949, *Rev. Sci. Instrum.*, **20**, 36 ; 1950, *Ibid.*, **21**, 96.
Kerwin, L., and Geoffrion, C., 1949, *Rev. Sci. Instrum.*, **20**, 381.
Korsunsky, M., 1944, *J. Exp. Theor. Phys. USSR*, **14**, (2) 459 (in Russian; English version, 1945, *J. Phys., USSR*, **9**, 14).
Korsunsky, M., Kelman, V., and Petrov, B., 1944, *J. Exp. Theor. Phys. USSR*, **14**, (10–11), 394 (in Russian); English version, 1945, *J. Phys. USSR*, **9**, (1), 7.
Ploch, W., and Walcher, W., 1950, *Z. Phys.*, **127**, 274.
Siday, R. E., 1947, *Proc. Phys. Soc.*, **59**, 905.
Smythe, W. R., Rumbaugh, L. H., and West, S. S., 1934, *Phys. Rev.*, **45**, 724.
Spighel, M., 1949, *J. Phys. Radium*, **10**, 207.
Stephens, W. E., 1934, *Phys. Rev.*, **45**, 513.

Measurements of the Electron-Optical Properties of Solenoid Prisms*

By W. EHRENBERG and J. C. E. JENNINGS
Birkbeck College, Malet Street, London W.C. 1

MS. received 8th October 1951

ABSTRACT. Cathode rays were deflected and focused in the median plane between a pair of similar coaxial solenoids. Foci free of quadratic aberration were found at all pole separations and ratios of electron momentum to field strength, when the impact parameters of the electrons were suitably selected. This property would enable a spectrum to be photographed with fairly uniform quality over a considerable range of $H\rho$. The loci of these foci were found. Values of the aberration coefficients and of the dispersion are given.

§ 1. INTRODUCTION

In order to supplement the analytical and computational studies of axially symmetric magnetic prisms made by Siday (1947) and Jennings (1952, to be referred to as I) and to obtain specific data, a solenoid prism with variable pole separation was constructed and its deflecting and focusing properties were investigated by means of cathode rays, which were observed on a movable fluorescent screen (fig. 1).

---

* This paper includes material from Part III of a thesis (1950) by J. C. E. J. which has been approved by the University of London for the degree of Ph.D. It is referred to in the text as 'Thesis'.

§ 2. EXPERIMENTAL ARRANGEMENT

A coaxial pair of iron-free solenoids was used, because the return yoke of an iron prism would have spoiled the axial symmetry, and it was desired that the field should relate as closely as possible to that for which calculations had been made and to which the theory of I applied. Further, the field of a pair of cylindrical iron pole pieces differs appreciably from that of ideal uniform circular plane poles on account of flux leakage. Iron-free solenoids, on the other hand, have the disadvantage of remote poles equal and opposite to the principal poles between which the prism field is produced. These remote poles considerably affect the rays far from the axis of symmetry. The solenoids were wound with four layers of 22 s.w.g. double cotton covered copper wire on water-cooled brass formers 5·0 cm in diameter and 20 cm long; at currents above 7 amperes the coils were additionally cooled by immersion in circulating oil. Each solenoid carried approximately 800 turns. Measurements were made by varying the current in the solenoids, the separations $2a\zeta$ (where $a = 2{\cdot}75$ cm, the mean coil radius) of their principal poles being 1·0, 3·6 and 7·2 cm, i.e. $\zeta = 0{\cdot}18$, 0·65 and 1·31. Since the $H\rho$ of the electrons was normally 340 gauss cm, $a\Psi \equiv aH_0/H\rho$ was numerically equal to $0{\cdot}328\,I$, $0{\cdot}179\,I$ and $0{\cdot}0800\,I$ respectively, where H_0 is the field at the intersection of the solenoid axis and the median plane, and I is the solenoid current in amperes.

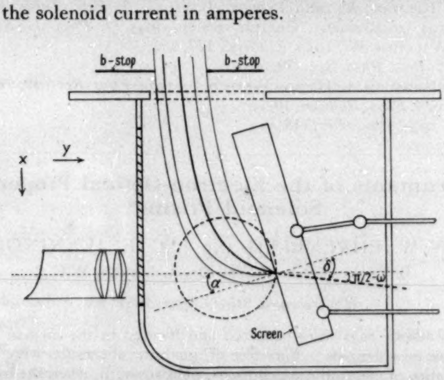

Fig. 1. Median section of deflection chamber. The broken circle is the outline of the solenoids. The principal ray is drawn as a bold line, its tangent at the focus is a broken line. The directions x and y correspond to the coordinates of fig. 4. Alternative screen supports allowed the whole relevant portion of the box to be swept by the screen.

The electron source was a hairpin filament of tungsten, so mounted that it could be displaced longitudinally and laterally with respect to the 3 mm aperture in the surrounding Wehnelt cylinder, which was maintained at an appropriate negative bias and which projected into a 5 cm diameter cylinder forming the anode of the electron gun. This cylinder terminated in a narrow rectangular brass box (fig. 1) lying between the principal poles of the solenoids. The cathode assembly, which was at −10 kv with respect to the approximately earthed anode, was 110 cm from the axis of the prism: thus the optical properties measured referred effectively to a source at infinity. The remoteness of the source gave the advantages (i) that a very small angle was accepted from the gun, so that the aberration of the source could be neglected, and (ii) that the prism formed a strongly demagnified image of the source, whose size did not exceed the resolution limit of the long-focus microscope used for observing the fluorescent screen of fine-grain willemite, on which the electron-optical image was formed. Tests made by scanning a fine spot across a similar willemite screen showed that its resolution limit was not more than $5\,\mu$; this was confirmed by the sharpness of the shadow thrown by crossed $10\,\mu$ wires just above the screen. The theoretical resolution limit of the microscope was $3\,\mu$ and in practice it was certainly better than $5\,\mu$. Figure 2 shows the construction of the microscope, for the optical design of which the authors are indebted to Dr. C. F. Dietrich of this College and of Optical Measuring Tools Ltd. The objective consisted of two 10 cm focal length achromats, each spherically corrected for infinity and the principal focus. The effect of the plano-concave aplanatic achromat was to produce in the plane of the eyepiece scale a four times magnified image of an object placed 10 cm in front of the objective. A 15 × eyepiece was used. Coplanar with the eyepiece scale a photographic film could be placed and rotated, after visual focusing, so as to enable up to three exposures to be taken.

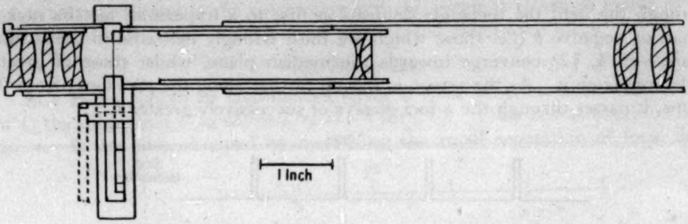

Fig. 2. Section through long-focus microscope, showing photographic film holder.

The cathode rays, being of fairly low momentum, were sensitive to stray magnetic fields. Since nearly the whole of their flight was almost parallel to the axis of the cathode-ray tube, this was set along the earth's total field (x direction of fig. 1). Preliminary experiments showed that magnetic fields from laboratory apparatus (rheostats, transformers, etc.) were scanning the electron beam at mains frequency. These disturbances were reduced to that of a steady field by pulse-modulating the electron beam in synchronism with the 50 c/s mains; the pulse length was about 1 millisecond. It may be remarked incidentally that pulse modulation makes possible the observation of fluorescent screens at high current densities without the risk of screen saturation; further, if the pulse repetition rate equals the mains frequency, the h.t. smoothing requirements are reduced.

In order to exhibit and measure dispersion and resolution, the 10 kv accelerating potential was modulated at 25 c/s by an amount $\delta V \leqslant 120$ volts. In the classical approximation, valid at 10 kv, $2V/\delta V = H\rho/\delta(H\rho)$. The phase relation of the 50 c/s pulse modulation on the grid of the electron gun to the 25 c/s square-wave modulation on the anode of the cathode-ray tube is shown in fig. 3.

§3. GENERAL CHARACTER OF PRISMATIC FOCUSING

This paper is chiefly concerned with the focusing of rays in the median plane between the solenoids. Any such ray, for a given momentum, is characterized by its 'impact parameter' b (i.e. the distance of its asymptotes from the axis of the solenoids) and it is convenient to refer to such focusing as 'b-focusing'. Rays outside the median plane are also focused in a surface normal to the median plane; this is called 'z-focusing'. Correspondingly, a stop limiting the parameter b is called a 'b-stop', one limiting displacement from the median plane a 'z-stop'. With the help of a narrow z-stop and a wide b-stop the general character of prismatic focusing can be observed. Suppose that the fluorescent screen (in fig. 1) is swung up towards the stops above the outline of the solenoids, by the use of a special set of screen supports; then the illuminated area is a rectangle long in the b, narrow in the z direction. As the screen is swung down through the field the rectangle deforms at first to a trapezium, for the rays of small or negative b (i.e. those which are most strongly deflected in the median plane—cf. I, §2) converge towards the median plane, whilst those of greater b diverge from it. As the screen is moved further along the rays away from the stops, it passes through the z-foci of rays of successively greater b.

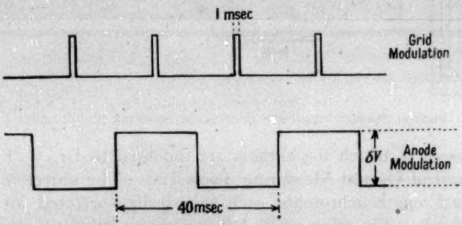

Fig. 3. Forms and phase relation of anode and grid modulations.

This picture is qualitatively true of the z-focusing over the whole range of prism currents and ray parameters investigated. It is, however, in practice complicated by the b-focusing, which is superimposed on it. If the range of b has been suitably selected, the trapezium becomes less elongated in the b direction and the intensity near the middle of its length builds up as the screen descends through the field. Eventually, this increase of intensity reaches a sharp peak, which is the cubic (cf. I, §1) focal line. It is characteristic of the cubic focus that the aberration pattern of the marginal rays lies on either side of it. If the screen descends still further, the bright line broadens and is soon seen as two bright lines with a region of fairly high intensity between them. Either of these lines, which are intercepts of the caustic curve (I, §7), may be selected by closing down the b-stop; the selected line then shows typical quadratic aberration, i.e. the marginal rays all lie on one side of it, as in the semicircular focuser.

The most unexpected result of our observations was that a cubic focus could be formed over a wide range of prism currents at each pole separation, provided that the range of b was suitably chosen. This discovery led to the theory of the thick prism (see I). As the prism current increases, the parameter b_{13} of the principal ray of the cubic focus decreases. Now the z-focusing action is increasingly converging as b tends in the negative direction, so that at a sufficiently high current (great enough Ψ) the z-focus of the family of rays b_{13} coincides with the cubic b-focus. Such a condition we describe as 'stigmatic focusing'; it is analogous to the 'double focusing' of Hedgran, Siegbahn and Svartholm (1950) and offers the possibility of fairly high light-gathering. It must be pointed out, however, that the z-focusing power varies with b, so that only the rays b_{13} are exactly at a stigmatic focus. Further, in the cases so far examined, stigmatic focusing is associated with rather high quartic aberration. The detailed discussion of z-focusing properties is, however, outside the scope of the present paper. It suffices to remark that little interest appears to attach to values of Ψ greater than that needed for stigmatic focusing, at any given pole separation.

§ 4. RESULTS

(i) *Locus of Cubic Foci*

Fig. 4 exhibits the loci of cubic foci for the three pole separations. The origin of coordinates is the prism axis and the incident electrons travel in the direction of positive x. Values of $a\Psi$ are marked along each locus.

(ii) *Dispersion*

If s is arc length in centimetres along a locus of cubic foci, then (cf. § 7 of I) the dispersion D is defined by $D = \Psi(ds/d\Psi)$. Thus D was obtained from fig. 4. It was also obtained by measuring the small separation of focal lines, occurring when the accelerating voltage was modulated by $\delta V = 120$ volts, and making allowance for the inclination of the fluorescent screen. The first method was probably the more reliable, although it involved graphical differentiation. In the modulation method the separation was only five to ten small divisions of

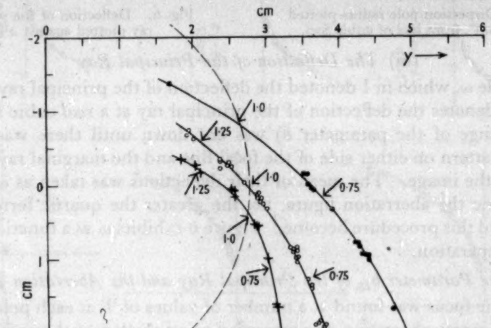

Fig. 4. Loci of cubic foci at three pole separations. The outline of the solenoids is shown as a broken circle. Values of $a\Psi$ are indicated by arrows at intervals along each locus.

the microscope eyepiece scale and could scarcely be read to less than one such division; the corrections involved ω, the angle of deflection of the principal ray b_{13}, which was not very exactly known (cf. fig. 6), as well as the inclinations of the screen and of the locus of cubic foci. In the result, the values of D from modulation were in most cases some 10% lower than those from the locus of cubic foci, which are shown in fig. 5, where the dimensionless form D/a is plotted against $a\Psi$.

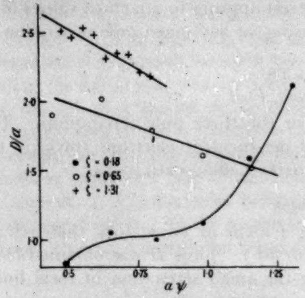

Fig. 5. Dispersion/pole radius plotted against $a\Psi$, from loci of cubic foci.

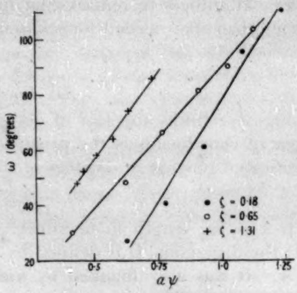

Fig. 6. Deflection of the principal ray plotted against $a\Psi$.

(iii) *The Deflection of the Principal Ray*

The angle ω, which in I denoted the deflection of the principal ray of a *virtual* focus, now denotes the deflection of the principal ray at a *real* cubic focus. The aperture (range of the parameter b) was cut down until there was no visible aberration pattern on either side of the focal line and the marginal rays were then traced near the image. The mean of their deflections was taken as ω. The less antisymmetric the aberration figure, i.e. the greater the quartic term, the more erroneous did this procedure become. Figure 6 exhibits ω as a function of $a\Psi$ for each pole separation.

(iv) *The Parameter b_{13} of the Principal Ray and the Aberration Pattern*

The cubic focus was found at a number of values of Ψ at each pole separation and the transverse aberration was measured as a function of the aperture, which was limited by b-stops some 6 cm from the axis of the prism (see fig. 1). The positions of the b-stops were related to b by measuring the deviation of the incident beam at the stops as a function of prism current and comparing this with the calculated effects of the principal and remote poles; the procedure is described in Thesis, Appendix 6. In agreement with the notation of eqns. (16) and (17) of I, the transverse aberration on the fluorescent screen was S_δ, δ being the angle between the principal ray and the perpendicular to the screen. The aberration measured by means of the microscope was $S_m = S_\delta \cos\alpha$, where α is the angle between the perpendicular to the screen and the axis of the microscope. Figure 7 shows S_m as a function of the aperture $b - b_{13}$. The parameter b_{13} of the principal ray was determined in the following way: it was assumed that

$$S_m = \tfrac{1}{2}h_3(b-b_{13})^3 + \tfrac{1}{2}h_4(b-b_{13})^4 + \tfrac{1}{2}h_5(b-b_{13})^5 + \ldots \qquad \ldots\ldots (1)$$

in conformity with the observed suppression of quadratic aberration and with eqns. (15) and (17) of I; S_m and b are measured in centimetres. Let S_{m+} denote

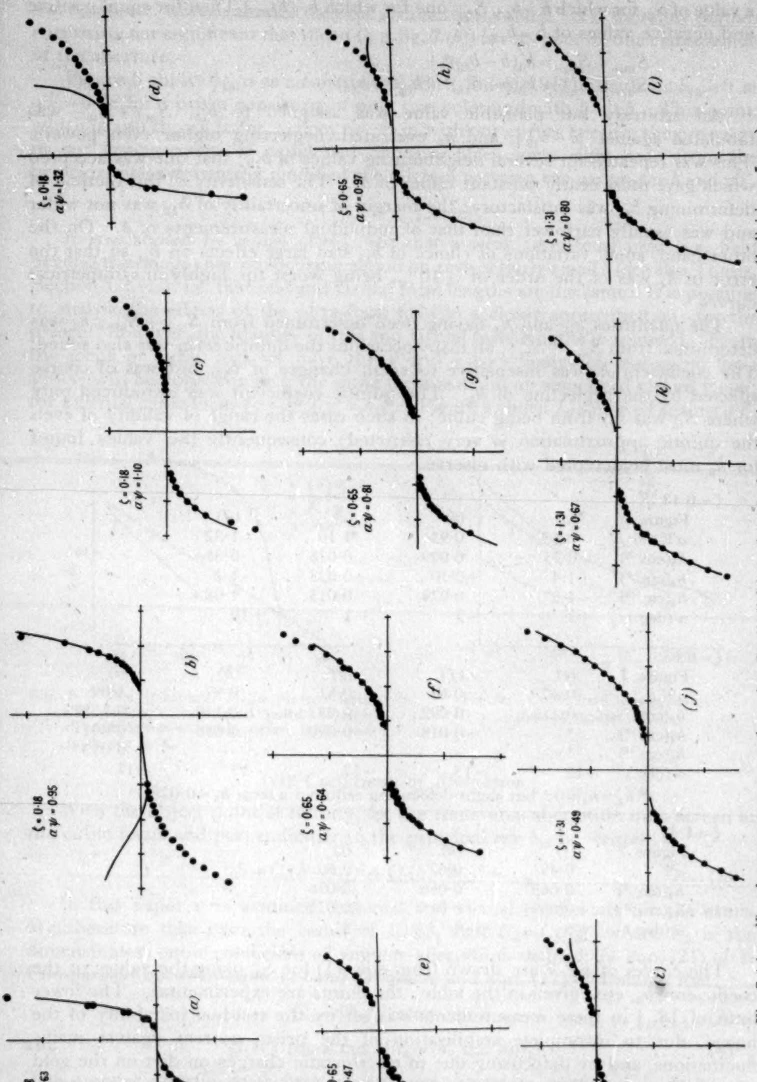

Fig. 7 (*a*) to (*l*). Apparent transverse aberration S_m (1 division = 1 mm) plotted against aperture $b-b_{13}$ (1 division = 5 mm). The points are experimental; the curves are from eqn. (1) with values of h_3, h_4, h_5 from table 1.

a value of S_m for which $b > b_{13}$, S_{m-} one for which $b < b_{13}$. Then for equal positive and negative values of $b - b_{13}$:

$$S_{m+} + S_{m-} = h_4(b - b_{13})^4 + \dots .$$
$$S_{m+} - S_{m-} = h_3(b - b_{13})^3 + h_5(b - b_{13})^5 + \dots .$$

An arbitrary but plausible value was assigned to b_{13}, $S_{m+} + S_{m-}$ was tabulated against $|b - b_{13}|$, and h_4 evaluated, neglecting higher even powers. This was repeated for several neighbouring values of b_{13}; that one was accepted which gave most nearly constant values of h_4. The sensitivity of this method of determining b_{13} was satisfactory: the margin of uncertainty of b_{13} was not wider and was usually narrower than that of individual measurements of b. On the other hand, small variations of choice of b_{13} had large effects on h_4, so that the error in h_4 was of the order of $\pm 10\%$, being worst for highly unsymmetrical curves.

The quantities b_{13} and h_4 having been determined from $S_{m+} + S_{m-}$, h_3 was determined from $S_{m+} - S_{m-}$; on many occasions the quintic term was also added. The coefficient h_3 was insensitive to small changes of b_{13}, but was of course affected by the neglecting of h_5. The quintic coefficient was introduced only where S_m was far from being cubic; in such cases the range of validity of even the quintic approximation is very restricted; consequently the values found for h_5 must be accepted with reserve.

$\zeta = 0{\cdot}18$

Figure 7	(*a*)	(*b*)	(*c*)	(*d*)
$a\Psi$	0·63	0·95	1·10	1·32
$h_3(\text{cm}^{-2})$	0·75	0·099	0·028	0·38
$h_4(\text{cm}^{-3})$	+1·4	+0·10	−0·023	−1·2
$h_5(\text{cm}^{-4})$	1·2	0·024	0·015	1·08
α (deg.)	+2	+3	−1	+10

$\zeta = 0{\cdot}65$

Figure 7	(*e*)	(*f*)	(*g*)	(*h*)	(*i*)
$a\Psi$	0·47	0·64	0·81	0·97	1·09
$h_3(\text{cm}^{-2})$	0·113	0·092	0·083	0·110	0·138
$h_4(\text{cm}^{-3})$	*	−0·018	−0·020	−0·058	−0·091
$h_5(\text{cm}^{-4})$	*	—	—	—	0·013
α (deg.)	−12	−15	−17	−17	−17

* $h_4 = h_5 = 0$; but slight defocusing required a term $h_1 = 0{\cdot}028$.

$\zeta = 1{\cdot}31$

Figure 7	(*j*)	(*k*)	(*l*)
$a\Psi$	0·49	0·67	0·80
$h_3(\text{cm}^{-2})$	0·069	0·066	0·076
$h_4(\text{cm}^{-3})$	−0·0095	−0·015	−0·023
α (deg.)	−5	−4	−5

The curves of fig. 7 are drawn from eqn. (1) for S_m using the values of the coefficients h_3, etc., given in the table; the points are experimental. The lower limit of $|S_m|$ in these measurements was set by the residual instability of the image, due to incomplete stabilization of the prism current against mains fluctuations, and by defocusing due to electrostatic charges on dirt on the gold stops. The upper limit of $|S_m|$ was set by the field of view of the microscope. Where h_4 was large, therefore, the aperture was highly unsymmetrical about b_{13}, but h_3, h_4, etc. were evaluated only for symmetrical values. It is therefore neither surprising nor significant that the fit (e.g. fig. 7 (*b*)) is very poor on one extreme side of the aperture.

Figure 8 shows b_{13}/a as a function of $a\Psi$. Siday (1947) calculated $b_{13}=0$ at $a\Psi=0{\cdot}88$ for a prism consisting of only two poles and with $\zeta=0{\cdot}5$. This point, which is also shown in fig. 8, does not fit in with our curves because the presence, in our arrangement, of equal and opposite poles some eight radii from the principal poles drastically modified the relation between the parameter b and $a\Psi$.

(v) *Focal Length*

It was shown by Siday (1947, §6) that a weak ultra-focal field (i.e. field beyond the image) has no focusing action on rays of fairly small b (see also Thesis, Section I.2.4.3), i.e. that real and virtual focal lengths are the same. It is possible to analyse the effects of the ultra-focal field to a closer approximation; for the present, however, the identity of real and virtual focal lengths is assumed. From the locus of cubic foci we have the x and y coordinates of real cubic foci; x^2+y^2 will be approximately the same for a real and an associated virtual focus; for a virtual cubic focus $f_3{}^2=x^2+y^2-b_{13}{}^2$. Figure 9 shows f_3/a plotted against $a\Psi$.

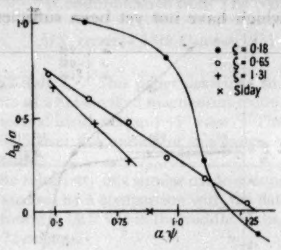

Fig. 8. The parameter b_{13}/a plotted against $a\Psi$. Siday's calculated point ($b_{13}/a=0$, $a\Psi=0{\cdot}88$) for a 2-pole prism with $\zeta=0{\cdot}5$ is shown as ×.

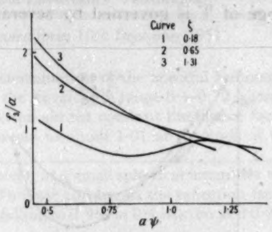

Fig. 9. Cubic focal length/radius plotted against $a\Psi$.

(vi) *Coefficients of Aberration*

With the object point at infinity, let the transverse aberration on a screen at the cubic focus and perpendicular to the principal ray b_{13} be written

$$S=C_t(b-b_{13})^3+Q_t(b-b_{13})^4+\ldots \qquad \ldots\ldots(2)$$

In this paper it is assumed that real and virtual coefficients are the same. We therefore take over the result of I, §3, that $C_t=C_3/f_3{}^2$, where C_3 is the dimensionless cubic coefficient of angular aberration, defined by eqn. (21) of I. Comparison between eqns. (1) and (2) above and eqn. (17) of I shows that

$$C_3=\tfrac{1}{2}h_3f_3{}^2\sec\alpha\cos\delta \qquad \ldots\ldots(3)$$

and

$$Q_t=\tfrac{1}{2}\sec\alpha\cos\delta[h_4-(h_3\tan\delta)/f_3]. \qquad \ldots\ldots(4)$$

The angular quartic coefficient is not given, since, as remarked in I, §3, its relation to the transverse coefficient is complicated when cubic aberration is present.

Figures 10 and 11 show the dimensionless quantities C_3 and a^3Q_t respectively as functions of $a\Psi$.

(vii) *z-Focusing*

Stigmatic focusing (see §3 above) occurred at $a\Psi \simeq 1{\cdot}3$ for $\zeta = 0{\cdot}18$, at $a\Psi \simeq 1{\cdot}6$ for $\zeta = 0{\cdot}65$ and at $a\Psi \simeq 1{\cdot}2$ for $\zeta = 1{\cdot}31$.

(viii) *Resolution*

Measurements were frequently made of the smallest modulation of the accelerating voltage needed for the corresponding focal lines to be visibly resolved in the microscope. On a number of occasions the observed resolving power, according to this criterion, reached $H\rho/\delta(H\rho) = 10^4$. This was in agreement with the source size of about 200 μ, the magnification ratio and the dispersion (fig. 5). It may be remarked that the resolution of two lines of equal intensity is little affected by cubic aberration.

§ 5. DISCUSSION OF RESULTS

The most important result is the existence at all pole separations of a locus of cubic foci with Ψ as parameter. This makes the instrument a *spectrograph* and in this sense the first improvement on the semicircular focuser. The usable range of Ψ is governed by several factors which have not yet been sufficiently investigated; of these the most important, at least in β-spectroscopy, is the z-focusing. To determine the relation between 'luminosity' (Geoffrion 1949) and resolving power it is necessary to consider the imagery of a source of considerable extent parallel to the axis of symmetry, as well as to know the dispersion and the transverse aberration on a screen tangential to the locus of cubic foci. The measurements which we have made show that, especially at close pole separations, the quartic and higher coefficients of aberration are large at the stigmatic focusing condition. It must be borne in mind, however, that both b-focusing and z-focusing properties are functions of the magnification. As regards the former, the functional dependence has been established in I for virtual imagery. If the action of the ultra-focal field can be calculated, therefore, the present results will become applicable to all magnifications.

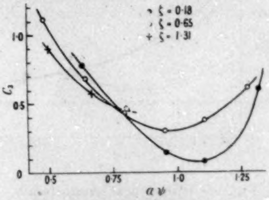

Fig. 10. Cubic aberration coefficient C_3 plotted against $a\Psi$.

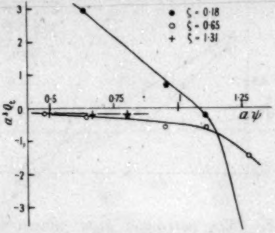

Fig. 11. Quartic aberration coefficient a^3Q_t plotted against $a\Psi$.

ACKNOWLEDGMENTS

The work described in this paper was carried out in the Research Laboratory, Birkbeck College, University of London (director, Professor J. D. Bernal).

One of the authors (J. C. E. J.) acknowledges the receipt of a maintenance grant from the Ministry of Education under the Further Education and Training

Scheme. Part of the work was carried out during his tenure of a research assistantship provided by the Department of Scientific and Industrial Research under a scheme directed by Mr. R. E. Siday for the development of high precision β-spectroscopy.

The authors wish to thank Mr. R. E. Siday, from whose work the problem originated, for many valuable discussions.

REFERENCES

GEOFFRION, C., 1949, *Rev. Sci. Instrum.*, **20**, 638.
HEDGRAN, A., SIEGBAHN, K., and SVARTHOLM, N., 1950, *Proc. Phys. Soc.* A, **63**, 960.
JENNINGS, J. C. E., 1952, *Proc. Phys. Soc.* B, **65**, 256 (referred to as I).
SIDAY, R. E., 1947, *Proc. Phys. Soc.*, **59**, 905.

The Spectral Reflection Characteristics of a Smoked Magnesium Oxide Surface

BY G. W. GORDON-SMITH
(Communication from The National Physical Laboratory, Teddington)

MS. received 18*th October* 1951 *and in amended form* 10*th December* 1951

.B
5
2

ABSTRACT. This paper describes an absolute determination of the spectral luminance factors of a flat smoked magnesium oxide surface, in the wavelength range 0·4–0·72 micron, for normal incidence and 45° view. The results give an almost constant luminance factor of 1·005 over the middle of this range, with an increase to about 1·01 at the ends of the spectrum.

The selectivity of a similar oxide coating on the interior of a small spherical integrator was also studied by a comparison with the flat surface. In these conditions the reflection factor was found to be 0·975 in the middle of the spectrum, falling to 0·962 at 0·4 micron and 0·972 at 0·72 micron.

The coatings were fresh, of thickness just over 1 mm, and made from the smoke of burning magnesium ribbon. A photoelectric method was used, and problems connected with the linearity of the photocell characteristic and with the spectral transmission of the monochromator used were examined and are discussed. Adequate references are given to various earlier investigations.

§ 1. INTRODUCTION

FOLLOWING a resolution passed by the Commission Internationale de l'Eclairage in 1931*, magnesium oxide when illuminated at 45° incidence and viewed normally has been accepted as a standard white surface whose luminance factor could be taken as unity, and spectral selectivity as insignificant, for most practical purposes.

Many studies of magnesium oxide have been made (Pfund 1920, Preston 1929–30, Priest and Riley 1930, Gibson and Keegan 1938, Benford, Lloyd and Schwarz 1948, Middleton and Sanders 1951), but there is no record of a *direct* measurement of selectivity under the prescribed conditions of unidirectional incidence and reflection. In the present work these conditions were observed, except for an interchange of the directions of illumination and view. In this way it was easier to obtain uniform illumination over the necessary area of the surface, while, by the principle of optical reversibility, the results should be unaffected by the change.

* *C.I.E. Compte Rendu des Séances*, Cambridge, 1931, p. 23.

Measurements were also made of the selectivity of a spherical integrator coated internally with magnesium oxide. The results are given, and also values deduced from them for the spectral reflection of the oxide surface under the diffuse conditions of illumination prevailing in the integrator.

§ 2. MEASUREMENT OF THE SELECTIVITY OF A FLAT SURFACE OF MAGNESIUM OXIDE

The spectral energy distribution of the incident light and of that reflected from the magnesium oxide surface after dispersion by a single monochromator were compared directly by a photoelectric method. The monochromator used was a Hilger–Tutton instrument. Double monochromators or stray-light filters were unnecessary, the spectral energy distributions compared being very nearly alike. For the same reason a large bandwidth was permissible, the slits being fixed and giving a total bandwidth of 0·018 micron at 0·58 micron. The emergent light was measured with a Cintel VB 39 vacuum photocell, a type designed specially for photometric measurement. This was followed by a simple d.c. amplifier, the signal from the photocell being balanced out and measured by a calibrated potentiometer in the input circuit. For the investigation on the flat oxide surface a 230 volt, 1 500 watt tungsten filament lamp operated at 150 volts was used. For direct measurements on the lamp (hereafter called condition (*a*) for brevity) the filament was situated on the optical axis of the monochromator, 30 cm from the entrance slit, and the photocell readings of the emergent light were taken at intervals of 0·02 micron through the spectrum. For measurement of the light reflected from the oxide (condition (*b*)), the surface was set at 45° across the axis, intersecting it at 20 cm from the slit. The lamp filament was 8 cm from the surface on the normal through the intersection of the axis with the surface. A similar set of readings was taken.

Ideally, the ratios of the two sets of readings, wavelength by wavelength, would give the required curve of relative spectral luminance factors. In practice it was necessary to satisfy two vital requirements not hitherto mentioned. First, in case of local variations in spectral response over the cell cathode, it was essential that the distribution of light on the cathode should be exactly the same in conditions (*a*) and (*b*). The exit slit was therefore imaged on the cathode with a suitable lens. Secondly, it was essential that the relative spectral transmission of the monochromator should be sensibly the same in condition (*b*) as in condition (*a*). To this end, it was necessary to make the effective aperture of the instrument as nearly as possible the same for the two conditions, and, even then, to make some tests for similarity of spectral transmission. The slit height was therefore set at 2 mm to restrict the upper and lower diffuse edges of the slit-image of the filament formed in the aperture (condition (*a*)) and so also to reduce its overall vertical extent. A stop 15 mm square was then placed over the telescope lens; this was just large enough to accept the whole area of this image, with a 1 mm safety margin, but cut off the peripheral part of the aperture which otherwise would have been effective in condition (*b*) but not in condition (*a*). The lamp was at the stated distance of 30 cm from the entrance slit. The position of the lamp image within this stop, for condition (*a*), could be seen, for adjustment and centring, by placing the eye at the image of the exit slit reflected to one side, for convenience, by a prism.

.B
5
2

§ 3. THE SPECTRAL TRANSMISSION OF THE MONOCHROMATOR

A preliminary experiment with the stop removed, and the lamp 'image' displaced laterally by 10 mm on either side of the axial position, gave the results shown in curves 1 and 2 of the figure. The ordinates represent the ratios of transmissions effective for the two lateral positions to those for the axial position. The changes in transmission in the green are small. At the ends of the spectrum, however, where the prism had a higher absorption, the transmission changes by some 10% for a 10 mm displacement of the light-beam in the aperture. This indicated a marked change in the effective relative spectral transmission of the optical train. Evidently, then, inaccurate centring of the beam in the square stop, in the main experiment, might involve a measurable change. A similar check was therefore made, in which the beam was deliberately de-centred by about 1 mm on either side of the axial position—the maximum range allowed by the stop, by reference to whose outline the displacements were now judged. The ratios of transmissions for one off-axis position to those for the other are shown in curve X in the figure. (Note: This curve should not intersect one for a 10 mm displacement. The reason for its doing so is probably a slight inadvertent change in lamp distance when making a lateral displacement which affected all the ordinates of one of the curves in a constant ratio.)

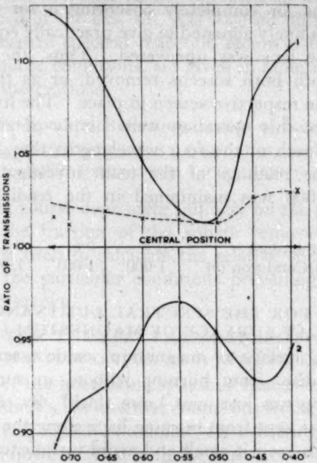

Spectral transmission of monochromator for non-central elements of the aperture relative to central values. Curve 1. 10 mm off centre, path through prism diminished. Curve 2. 10 mm off centre, path through prism increased. Curve X. Ratio of values for two opposite displacements each 1 mm off centre.

It is seen that a centring uncertainty of ±1 mm would involve uncertainties in relative spectral transmission of rather more than ±0·5% at the ends of the spectrum. With the aid of the observing arrangement described, the precision of centring was in fact well inside these limits.

These tests, however, afforded no *direct* check on whether the spectral transmission for the *centred* lamp 'image' (condition (*a*)) was exactly the same as when the 15 mm stop was filled with light from the oxide surface (condition (*b*)). Nevertheless, the results, considered together with the known structure of the 'image' and its averaging effect, enabled an approximate estimate to be made of the possible differences in relative spectral transmission as between the two cases. These did not appear to exceed one quarter per cent, expressed as a differential between transmissions at the ends and at the middle of the spectrum.

§ 4. LINEARITY OF RESPONSE OF THE PHOTOCELL

As a necessary precaution the relationship between photocell response and incident light intensity was also checked, at four wavelengths, since the optical limitations already mentioned imposed a ratio of about 30 : 1 on the readings for conditions (*a*) and (*b*) respectively. The method of addition was used. By measuring two nominally equal intensities first separately, and then when incident simultaneously on the cell, a 'linearity correction' for the ratio 2 : 1 was found. Repetition of this, at four more levels, covered the ratio of about 30 : 1. The monochromator aperture was filled with light by using a suitable lamp and condenser to illuminate the entrance slit. Over the telescope lens was fixed a narrow horizontal diametral bar against which the edges of two black opaque screens could be placed cutting off light from either the upper or lower half of the lens, or completely obscuring it for a zero-reading. The position of the bar was finely adjusted to give practically equal photocell readings whichever half of the lens was uncovered. Thus, the total light could be measured directly, with both screens removed, or as the sum of two equal readings, each with the respective screen in place. The five increasing intensity levels for repetition of this operation were simply obtained by adjusting the lamp voltage, and at each of the four wavelengths they were set to cover the corresponding extreme readings of the main investigation. A precision of about 5 parts in 10 000 was maintained in the readings and the ratios of sensitivities were

Wavelength (microns)	0·7	0·6	0·5	0·4
Condition (*a*)/Condition (*b*)	1·000	1·001	1·003	1·005

§ 5. RESULTS FOR THE SPECTRAL LUMINANCE FACTORS OF A FLAT SURFACE OF MAGNESIUM OXIDE

A freshly smoked surface of magnesium oxide was then prepared on a silver-plated copper disc, from burning ribbon, in surroundings free from draughts. The coating was just over 1 mm thick. By repeated extinction the flame of the ribbon was kept from burning back along the ribbon for more than about 2 cm, in order to keep it small and avoid turbulence in the rising stream of oxide; it was not allowed to approach the surface being coated. The results obtained for the spectral luminance factor are given in table 1. They are the mean values of six sets of observations at intervals of 0·02 micron, with six additional sets at wavelengths 0·7, 0·6, 0·5 and 0·4 micron only. The absolute luminance factor for white light probably lies between 1·00 and 1·01 (Preston and Gordon-Smith 1952); the relative spectral values as now measured have therefore been set out on a scale consistent with a white light value of 1·005. They may thus be taken as absolute values to within about 0·5%. They have been corrected for the differential non-linearity of the photocell characteristic, but have not been smoothed.

Table 1. Absolute Luminance Factor of Magnesium Oxide for Normal Incidence, 45° View

Wavelength (microns)	0·72	0·70	0·68	0·66	0·64	0·62	0·60	0·58	0·56	0·54	0·52	0·50	0·48	0·46	0·44	0·42	0·40
Luminance factor	1·011	1·010	1·010	1·007	1·007	1·005	1·005	1·005	1·005	1·005	1·005	1·006	1·007	1·007	1·007	1·008	1·015

§ 6. MEASUREMENT OF THE SELECTIVITY OF MAGNESIUM OXIDE IN AN INTEGRATING SPHERE

For measurements in the integrating sphere, the inside of a silver-plated copper sphere 10 cm in diameter was coated to a thickness of about 1 mm. One circular hole of 25 mm diameter admitted light from a lamp, while another of 20 mm diameter allowed the monochromator to receive light from a part of the sphere wall not directly illuminated by the lamp. The standard of comparison was not now a bare lamp, but the flat oxide surface just calibrated, set up as in the first investigation. In this comparison, then, the entrance slit always viewed an extended uniformly bright surface, and so the aperture of the monochromator was always uniformly filled. The 15 mm stop was therefore removed, the slit height increased to 6 mm, and enough light obtained from a more convenient smaller lamp of 100 volt 250 watt rating, operated at 90 volts. The aperture of the telescope, instead of the exit slit, was focused on the photocell cathode. The results for the relative spectral reflection factor of the sphere as a whole, under the stated geometric conditions, are given in table 2. They are the mean values of six sets of observations.

Table 2. Relative Spectral Reflection Factor of Experimental Sphere

Wavelength (microns)	0·72	0·70	0·65	0·60	0·55	0·50	0·45	0·40
Reflection factor	0·930	0·940	0·964	0·990	1·000	0·965	0·882	0·781

These results are of course dependent not only on the properties of the oxide coating but also on the fraction of the sphere removed to make the holes. However, they may be used to calculate the relative spectral reflection factors for the oxide, under the particular conditions prevailing in the sphere, if the areas of the holes are known.

§ 7. RESULTS FOR THE SPECTRAL REFLECTION FACTORS OF MAGNESIUM OXIDE AS A SPHERE COATING

The usual theory of the integrating sphere is based on the assumptions that the coating obeys Lambert's law and that conditions in the sphere are completely diffuse. These hold very closely, no doubt, for a coating of magnesium oxide. It is worth remarking, however, that both the first incident light, and the sample finally taken by the monochromator were restricted very nearly to the normal to the wall surface, and also that at very oblique angles smoked magnesium oxide exhibits specular reflection for the longer wavelengths preferentially. Strictly ideal conditions are not therefore achieved, either as regards diffusion in the sphere, or as regards the precise definition of what is being measured, but they must be assumed in what follows.

The monochromatic radiation reflected from an element of the sphere wall is proportional to $K\rho_\lambda^2/(1-\theta\rho_\lambda)$ where ρ_λ is the reflection factor under consideration (diffuse incidence and diffuse reflection) for wavelength λ, K is a factor proportional to the radiation of that wavelength entering the sphere, and

θ is the fraction of sphere wall remaining after allowance for holes, in this case 0·974. This formula applies to any portion of the wall not receiving the first incident radiation from the source. The problem is then to find a set of values of ρ_λ through the spectrum which gives values of $\rho_\lambda^2/(1-\theta\rho_\lambda)$ bearing a constant ratio to the results of table 2 and which also gives the correct value for the white-light reflection factor under sphere conditions, which is known to be very close to 0·975 (Preston 1929–30). This set of values is given in table 3.

Table 3. Absolute Diffuse Spectral Reflection Factor of Magnesium Oxide in an Integrating Sphere.

Wavelength (microns)	0·72	0·70	0·65	0·60	0·55	0·50	0·45	0·40
Reflection factor	0·972	0·972	0·973	0·975	0·975	0·973	0·969	0·962

§ 8. DISCUSSION OF RESULTS, AND CONCLUSIONS

The results for the flat surface confirm that 1 mm thickness of smoked magnesium oxide is in fact very nearly non-selective under the standard conditions. The observed increases in luminance factor toward the ends of the visible spectrum exceed the estimated probable error, but only by a little. The results for the diffuse reflection factors in an integrator agree remarkably well with those of Middleton and Sanders (1951). Taken together with Middleton and Sanders' work, the present investigation tends further to confirm that the reproducibility of a fresh surface smoked carefully and slowly with burning ribbon is better than has been thought, and also perhaps than that given by the recommended procedure of the National Bureau of Standards (1939, 1949). There now seems no doubt that the colour of a smoked coating 1 mm thick in the sphere is somewhat green.

It is a criticism of the present work that measurements have not been made on more than one sample, but experience at the National Physical Laboratory over many years, with fresh coatings made as described, and of about the same thickness, has not provided evidence of any serious variations. To avoid ageing effects as well, it would now seem necessary to protect coatings from the action of carbon dioxide* and of ultra-violet radiation (Middleton and Sanders 1951), and probably also of moisture. Further work on the chemical and photochemical changes produced by these agents might be profitable. Whether measurements on greater thicknesses would be so, is doubtful.

ACKNOWLEDGMENT

The work described above has been carried out as part of the research programme of the National Physical Laboratory, and this paper is published by permission of the Director of the Laboratory.

REFERENCES

Benford, F., Lloyd, G. P., and Schwarz, S., 1948, *J. Opt. Soc. Amer.*, **38**, 445.
Gibson, K. S., and Keegan, H. J., 1938, *J. Opt. Soc. Amer.*, **28**, 372.
Middleton, W. E. K., and Sanders, C. L., 1951, *J. Opt. Soc. Amer.*, **41**, 419.
National Bureau of Standards, 1939, *Letter Circular No.* 547; 1949, *Circular No.* 484.
Pfund, A. H., 1920, *J. Franklin Inst.*, **189**, 379.
Preston, J. S., 1929–30, *Trans. Opt. Soc.*, **31**, 15.
Preston, J. S., and Gordon-Smith, G. W., 1952, *Proc. Phys. Soc.* B, **65**, 76.
Priest, I. G., and Riley, J. O., 1930, *J. Opt. Soc. Amer.*, **20**, 156.

---

* Unpublished work at N.P.L. indicates the formation of some 5% of carbonate in coatings exposed to saturated CO_2 for 24 hours.

Low-frequency Noise Spectra of Hot-filament Low-pressure Discharge Tubes

By H. MARTIN and H. A. WOODS[*]
Queen's University, Belfast

Communicated by K. G. Emeléus; MS. received 8th November 1951

ABSTRACT. Measurements have been made of the low-frequency noise spectrum of a number of hot-cathode discharges in mercury vapour saturated at room temperature. As previously reported by Cobine and Gallagher, the spectrum is continuous, with superposed peaks. The latter can be partly attributed to harmonic components of ionic relaxation oscillations. The upper frequency limit of the continuum exceeds 10 Mc/s in some instances. Most of the noise from the tubes studied originated near the cathode. Some relations have been traced between the noise and oscillations and position on the current–voltage characteristic curve for the tube, but there is variation from one tube to another.

§1. INTRODUCTION

Few systematic observations have been reported on the low-frequency electrical noise and oscillations emanating from hot-cathode discharge tubes containing gas at low pressure. The most comprehensive measurements of noise spectra have been made by Cobine and Gallagher (1947 a, b), who found that above a critical frequency, which depended on the gas used, the noise amplitude decreased rapidly with increase in frequency. Massey (1949) and his collaborators and Armstrong, Emeléus and Neill (1951) also report work on noise.

The present investigation was done with the aims of (i) studying the effect on the noise and oscillations of introducing different internal structures into the discharge, and of using different tubes; (ii) finding how the noise varies with position on the current–voltage characteristic of a tube; (iii) finding the upper frequency limit, if any, beyond which noise is absent.

The results indicate that the phenomena are general, and present with all internal structures. Moreover, the noise generated between the anode and cathode is very dependent on the point on the characteristic at which it is measured. The upper limit of the noise spectrum is in certain cases greater than 10 Mc/s. In many instances the noise originates at the cathode or in a region near it.

§2. EXPERIMENTAL ARRANGEMENTS

Three tubes were used, two of which were demountable. The first (fig. 1 (*a*)) had a hemi-cylindrical nickel anode A, 5 cm long and 1·1 cm in radius, and an axial filament of 200 μ tungsten wire all mounted on one pinch. A second hemi-cylinder could be held in place over the open part of the anode by means of two end caps, giving effectively a totally enclosed filament. These electrodes were mounted in a glass envelope 23 cm long and 4·4 cm in diameter. The second (fig. 1 (*b*)), which was also demountable, had a nickel disc anode A, spaced 18·9 cm from a coiled tungsten filament F, in a glass tube 5·4 cm in diameter.

---

[*] Musgrave Student in Physics.

Different auxiliary structures could be introduced into the interelectrode space. Both tubes were continuously pumped and roughly thermostated. The third tube, a G.U.50 valve, was a sealed-off mercury vapour rectifier with a cap-shaped anode, the hollow side of which faced a filament composed of two crinked metal strips wired in series. All three contained mercury vapour saturated at about 20° c.

The circuit for obtaining the noise spectra was connected directly between the anode and the cathode of the discharge tubes. It was almost identical with a superheterodyne circuit used by Cobine and Curry (1946), except that in the present work, instead of using an audio-frequency sound analyser to measure the noise amplitude, the attenuation necessary to bring the mean width of the trace on an oscillograph connected to the output to a fixed value was taken as a measure of the noise. The noise amplitude calibration of this apparatus was made against a G.P.O. R I No.1 Measuring Set. In addition, a few measurements were made using the G.P.O. apparatus as a field-strength meter, one end of a length of wire being wound a few times round the outside of the tube and the other connected to the G.P.O. apparatus. This acted as an aerial, but as it was not of the standard form for the meter the readings obtained were not absolute. The first circuit covered the range from 14 kc/s to 2 Mc/s, while the G.P.O. set was used for measurements up to 11 Mc/s.

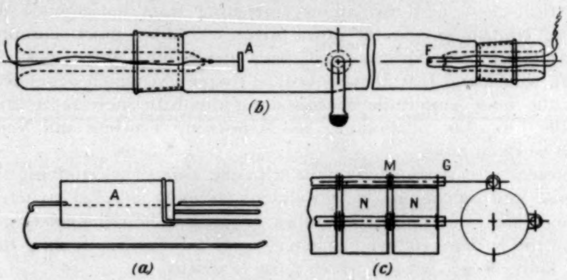

Fig. 1. Discharge tubes. (*a*) Electrode structure of tube 1, anode A, viewed laterally. (*b*) Electrode structure of tube 2; the projection is a side tube containing liquid mercury. (*c*) Nickel ring interelectrode structure for tube 2—left, longitudinal section; right, transverse section; N, nickel rings, G, glass supporting rods, M, mica spacers.

The tube circuits were conventional, and employed only batteries for high and low tension. All the apparatus used was enclosed in an electrostatic screening cage. Large chokes placed in the anode and filament leads prevented any disturbances, which might have been present despite the cage, from reaching the tube. The pump motor for the vacuum train was placed outside the cage. Microphonics were reduced to a minimum by suitable valve-holders and by surrounding the valves with cotton wool. Care was also taken that the batteries used were stable. By these means the background noise was reduced to a value such that no deflection was observable on the cathode-ray oscillograph screen with the maximum gain. The noise amplitude was expressed in decibels relative to a zero level of $10\,\mu\text{v}/(\text{kc/s})^{1/2}$, which was that used by Cobine and Gallagher. In the present work the least noise amplitude detectable was about 20 db on this scale.

§ 3. EXPERIMENTAL RESULTS

The details varied for each run, but the general results were always the same, even for the three different tubes. Observations were made as the voltage across the tube was increased from zero to the maximum, the tube current and voltage being noted at regular intervals and measurements of the noise level at certain selected frequencies also being made at numerous points, in conjunction with a thorough scan over the whole frequency range for any discrete oscillations superposed on the background noise. An oscilloscope connected directly across the discharge tube allowed continual observation of the output from the tube, and the display on its screen was used as a guide as to when to take noise measurements.

The left-hand side of fig. 2 (*a*) shows a characteristic obtained for tube 1, without the end caps, the operating conditions being filament current 4·8 A, filament voltage 6·95 V, mercury vapour pressure 9×10^{-4} mm. The other two curves in this figure show the amplitude of the noise for a mean band width of 2000 c/s centred around the frequencies 86 kc/s and 2 Mc/s, the points lettered corresponding to those on the characteristic. In the sub-plasma region, A to E, oscillations in the frequency range 20–40 kc/s were observed on top of small background noise. On the nearly vertical part of the characteristic the noise amplitude went through various maxima, ultimately falling to low values as saturation was approached. Typical noise amplitude–frequency spectra are shown in fig. 2 (*b*), for the points G, H and J. A decrease in noise amplitude with increase in frequency occurs in each of these, but only when the value of the noise amplitude

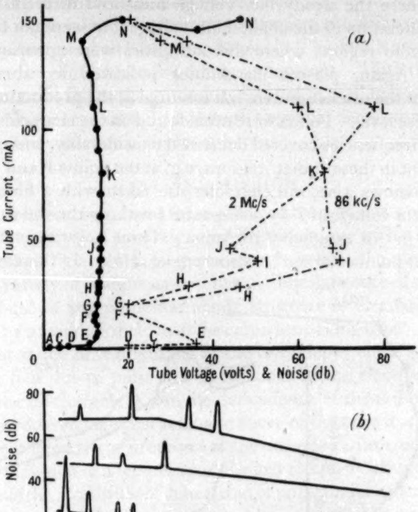

Fig. 2. (*a*) Current–voltage characteristics (left), and noise amplitude at 86 kc/s and 2 Mc/s (right) for tube 1; (*b*) noise spectra at selected points J top, G bottom.

was small at low frequencies did this bring the noise level down to the experimental zero of 20 db. The amplitude of the discrete oscillations observed varied widely over the characteristic, and their frequencies increased with anode current. No harmonically related oscillations were observed in the sub-plasma region, but above a tube voltage of 10–12 v even harmonics of different fundamental frequencies, as well as non-harmonically related oscillations, were recorded. However, oscillation frequencies greater than 100 kc/s were not obtained until the tube current reached at least 30% of its saturation value. Oscillations were less numerous as saturation was approached, but their frequencies were usually high, the maximum recorded being 1·20 Mc/s.

Similar experiments with a tube containing no ferromagnetic materials gave results of the same type, showing that the oscillations and noise were not due to amplification of a Barkhausen effect in the metal.

Throughout these experiments oscillations were often found at points on the characteristic where the steady d.c. voltage measured directly across the tube varied without alteration of the applied h.t. voltage, but were not confined at all to such places, nor to regions where discontinuities were apparent on the tube characteristics. Again, plasma instabilities indicated by abrupt changes in the appearance of the discharge were not essential to the production of oscillations or changes in noise level. Points were often found on the characteristics where the noise level at all frequencies covered decreased considerably, and oscillations were sometimes present in these 'quiet' regions, e.g. at the points F and G.

Figure 3 (*a*) shows a second characteristic taken with a filament current of 4·8 A and a filament voltage of 7·4 v, using tube 1 without the end caps, the mercury vapour pressure in this case being 10^{-3} mm. Three noise spectra taken with the G.P.O. set for the points marked are shown in fig. 3 (*b*). In this case no search was made for oscillation peaks. These measurements show that the noise spectrum can extend above 10 Mc/s. Only when the low-frequency value is small does the general decrease with frequency cause the noise level to approach the arbitrary zero for the recording apparatus.

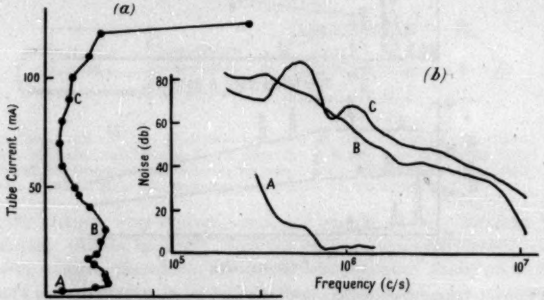

Fig. 3. (*a*) Current–voltage characteristic for tube 1; (*b*) noise spectra to above 10 Mc/s.

Throughout this work details varied for successive runs with the same anode and filament, possibly due to ageing of the latter. When different anode structures were used with the same filament for successive runs, the general features were also unchanged, though the details were again variable.

The large tube (fig. 1 (*b*)) was much more unstable then either of the others, the extent of the instability depending on the interelectrode structures. When the latter consisted of a series of insulated nickel rings (fig. 1 (*c*)) mounted so that the plasma could bulge between them, or spill behind the anode, the instability was much greater than when this was prevented by making the rings a press fit in a glass tube of diameter comparable with that of the anode. The instability was further diminished when no rings were present, and the plasma bounded by a glass tube of diameter 3·0 cm, set between the electrodes and a mica disc immediately behind the anode. This tube was never stable enough to obtain complete spectra, but oscillations were present, and also much noise with the same general form of spectrum as the other tube. If a small bar magnet was placed near the cathode the noise increased, whereas placing it near the anode did not affect the noise even when the volume of plasma changed markedly. This indicates that a large part of the noise is originating in some region near the cathode.

Using the G.U.50 valve under various operating conditions, oscillations were again observed superposed on background noise. The details again varied slightly for each run, but the general features remained constant. With this tube the noise level at all frequencies fell to the minimum detectable, well below saturation. No definite cut-off frequency was found, though the usual decrease in amplitude with increase in frequency was again always apparent.

§4. DISCUSSION

The results confirm in general those obtained by previous workers, and extend them in several respects. Low-frequency electrical noise with a broad continuous spectrum extending from audio frequencies into at least the megacycle region is generated by a variety of low-pressure tubes. The existence of the noise does not depend on the use of any particular anode structure or electrode material, and it can be affected by a magnetic field near the cathode of a long tube. The evidence is thus strong that much of it originates at the cathode, or close to it and, from the spectrum, that it is due to pulse-like fluctuations in the electron current leaving this region of the discharge. From the dependence of the noise on the operating point on the current–voltage characteristic curve of the tube it is probable that the fluctuations are related to the processes at the cathode surface, or in the gas near it, which precede emission of a temperature-limited electron current. This does not, however, exclude the possibility of generation of noise under other circumstances at the anode or, as in tube 2, with some internal structures, when a positive column is disturbed. There seems no reason why both types of noise should not coexist, or even be coupled by plasma waves (Armstrong, Emeléus and Neill 1951).

The discrete oscillations which have been found fall into two classes. The first occur with very small current densities, before a plasma has formed. This may be due to oscillations of positive ions in the potential minimum in the cathode sheath (Kingdon 1929). Since the minimum must exist along at least part of the cathode until complete temperature limitation of electron emission is reached with increasing cathode fall of potential, these oscillations may persist in the rapidly rising part of the characteristic, and be included amongst those then observed. The second occurs on the steep part of the characteristic curve, and is often, but not invariably, characterized by presence of overtones, with a preference for even harmonics. They are probably largely relaxation oscillations in which the discharge, or some part of it, is jumping abruptly, but with regular periodicity, between two almost stable configurations. The evidence points to those which have been recorded in this investigation having their origin near the cathode, but it is again possible for them to be generated near the anode (Armstrong, Emeléus and Neill 1951); the glare from the cathodes in the present investigation prevented visual observation of what was taking place in their immediate neighbourhood.

ACKNOWLEDGMENTS

The authors wish to thank the Research Laboratories of the General Electric Company, Wembley, for advice on the analysis of the noise spectrum and for a generous gift of much of the apparatus used for this purpose, and to thank Colonel H. B. Somerville for arranging for the loan of the G.P.O. Measuring Set. They are indebted to Professor L. F. Bates for pointing out the necessity for an experiment with a tube not containing ferromagnetic material. The problem was suggested by Professor K. G. Emeléus.

REFERENCES

Armstrong, E. B., Emeléus, K. G., and Neill, T. R., 1951, *Proc. R. Irish Acad.* A, **54**, 291.

Cobine, J. D., and Curry, J. R., 1946, *Rev. Sci. Instrum.*, **17**, 190.

Cobine, J. D., and Gallagher, C. J., 1947 a, *J. Appl. Phys.*, **18**, 110; 1947 b, *J. Franklin Inst.*, **243**, 41.

Kingdon, K. H., 1929, *Phys. Rev.*, **33**, 1075.

Massey, H. S. W., 1949, *Characteristics of Electrical Discharges in Gases*, ed. A. Guthrie and R. K. Wakerling (New York : McGraw-Hill).

A Thick-walled Ionization Chamber for Measuring the Intensity of X-Radiation of Energy up to 25 MeV

By B. H. FLOWERS*, J. D. LAWSON and E. B. FOSSEY
Atomic Energy Research Establishment, Harwell, Berks.

Communicated by D. W. Fry; MS. received 4th June 1951, *and in amended form 19th November* 1951

ABSTRACT. A thick-walled ionization chamber suitable for measuring the radiation intensity from synchrotrons and betatrons operating at energies up to 25 MeV is described. Calibration curves giving the current in the chamber per incident photon as a function of photon energy are given. The effect of wall thickness and secondary x-rays produced in the wall have been considered and included in the calculations. Experimental results consistent with the theory are described.

§1. INTRODUCTION

Previous calculations of the sensitivity of ionization chambers to x-radiation have usually been made assuming that there is a state of electronic equilibrium between the x-radiation and electrons in the chamber wall (Mayneord 1940, 1950, Fowler, Lauritsen and Lauritsen 1948). This assumption is valid for low energies where the range of the electrons liberated in the wall is small compared with the range of the X-ray quanta, but it is not correct for energies above about 10 MeV, where this condition does not hold. Empirical methods of correction have been suggested (Mayneord and Martin 1950), but in the present paper calculations for the energy range 1–25 MeV are made directly without assuming equilibrium conditions. The results are presented in the form of a graph of ionization current per cm^3 of air in the chamber against number of quanta falling per second on a square centimetre of the chamber as a function of quantum energy. Calculations of the overall sensitivity of the chamber to thin target bremsstrahlung radiation are also given for a few values of bombarding electron energy. Finally, a practical chamber is described and some experimental results are given.

---

* Now on temporary leave of absence at the Department of Mathematical Physics, The University, Birmingham.

§2. QUALITATIVE CONSIDERATIONS

The calculation will be made for a planar system consisting of a thick slab of material, in which, at a depth T, there is an air space of thickness ΔT. The electrons in the wall are produced mainly by Compton collisions and pair creation in the energy region of interest, but the photoelectric effect is of importance at lower energies. In addition, 'second order' electrons are produced by X-ray quanta degraded by Compton collisions, by bremsstrahlung from the 'first-order' electrons and by annihilation radiation. The ionization from these secondary electrons will be small, so that an approximate method of calculation may be used.

The ionization in the wall builds up to a maximum at a depth rather less than the range of the most energetic electron produced, and then dies away monotonically. Both for experimental reasons and because the calculation is simpler, the calibration has only been made for wall thicknesses greater than the range of the most energetic electrons.

The fraction of the incident energy converted to ionization per unit volume of the chamber wall as a function of depth will first be calculated, and the 'air equivalent' of the wall material will be found. It will then be possible to express the result in terms of the current per unit volume of air space per photon per unit area per sec.

The calculations refer specifically to aluminium-walled, air-filled, ionization chambers. The specific gravity and atomic weight of aluminium are assumed to be 2·7 and 27·0 respectively. All cross sections are those given by Heitler (1944). Energies, measured in MeV throughout, are expressed by the symbol W for photons, and by E for the *kinetic* energy of electrons (i.e. omitting the rest energy).

§3. CALCULATION OF CHAMBER CALIBRATION CURVES

3.1 *First Collisions*

First of all, the average fraction of quantum energy converted into ionization in a single collision of any kind must be found. Suppose a quantum of energy W produces by any means an electron of kinetic energy E, and let the fraction of electron energy which is ultimately dissipated in the form of ionization be $\eta(E)$, then the fraction of quantum energy converted directly to ionization is given by $(E/W)\eta(E)$. Let $\sigma(W,E)\,dE$ be the number having energies between E and $E+dE$, then the mean fraction of energy converted is given by

$$F(W)=\frac{\int(E/W)\eta(E)\sigma(W,E)\,dE}{\int\sigma(W,E)\,dE}. \qquad \ldots\ldots(1)$$

In order to calculate the function $\eta(E)$, the formulae given by Heitler (1944, pp. 173, 219) for rates of energy loss by collision and by radiation, $(dE/dx)_{\text{coll}}$ and

$(dE/dx)_{\rm rad}$ respectively, are used. In terms of these quantities, the fraction of electron energy E dissipated in ionization is given by

$$\eta(E) = \frac{\int (dE/dx)_{\rm coll}\, dx}{\int (dE/dx)_{\rm coll}\, dx + \int (dE/dx)_{\rm rad}\, dx}, \qquad \ldots\ldots(2)$$

where the integrations are to be taken over the whole range of an electron of energy E. From this expression η has been calculated numerically ; it is unity at low energies, dropping off slowly to 0·84 at 25 MeV as shown in fig. 1.

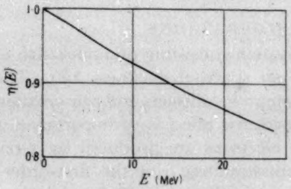

Fig. 1. Fraction of kinetic energy E of an electron converted to ionization in aluminium.

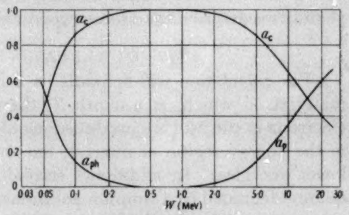

Fig. 2. Energy-dependence of the relative cross sections for photoelectric absorption $a_{\rm ph}$, Compton scattering $a_{\rm c}$, and pair production $a_{\rm p}$.

Equation (1) will now be split into its three component parts corresponding to the photoelectric effect, Compton scattering and pair production. In an obvious notation

$$\left.\begin{aligned} F &= a_{\rm ph}F_{\rm ph} + a_{\rm c}F_{\rm c} + a_{\rm p}F_{\rm p}, \\ \text{with}\qquad 1 &= a_{\rm ph} + a_{\rm c} + a_{\rm p}. \end{aligned}\right\} \qquad \ldots\ldots(3)$$

The coefficients a are the relative probabilities for the three processes given by the respective cross sections. Their energy dependence is shown in fig. 2.

The photoelectric process is of importance only at low energies where radiative losses are negligible. In this process, moreover, almost all the quantum energy is transformed into kinetic energy, so that $F_{\rm ph}$ is simply unity.

For the Compton effect we have

$$F_{\rm c}(W) = (1/W) \int E\eta(E)\sigma_{\rm c}(W,E)\, dE / \int \sigma_{\rm c}(W,E)\, dE, \qquad \ldots\ldots(4)$$

where $\sigma_{\rm c}(W,E)$ is given by the Klein–Nishina formula.

The pair production cross section is small for energies W less than about 2 MeV, and above this energy it is essentially independent of electron (or positron) energy. Thus a considerable simplification may be achieved by putting $\sigma_{\rm p}(W,E) = \sigma_{\rm p}(W)$ so that

$$F_{\rm p}(W) = \frac{2}{W(W-2mc^2)} \int_0^{W-2mc^2} E\eta(E)\, dE. \qquad \ldots\ldots(5)$$

In this last equation the additional assumption is made that radiative losses are the same for electrons and positrons, and this is true to a high degree of approximation.

The integrals $F_{\rm c}$ and $F_{\rm p}$ have been computed numerically, and $F(W)$ obtained from eqn. (3).

3.2. *Sensitivity of Chamber to First Collisions*

In the preceding section we have calculated the fraction F of quantum energy W which is converted into ionization by a single collision of any kind. We have now to inquire what ionization can be observed in the cavity of the chamber due to the passage through the wall of the initial x-ray beam. If unit intensity falls normally upon the front surface of the chamber, the intensity of the undeflected beam at a depth x cm is $\exp(-\tau x)$, where $\tau=\tau(W)$ is the total absorption coefficient for radiation of energy W. Moreover, if the electron range were zero, the fraction of energy converted to ionization in a thickness *dx at a depth x* would be

$$F\tau\exp(-\tau x)\,dx. \qquad \ldots\ldots(6)$$

To take into account the finite range of the ejected electrons we should consider rather the effect of an average intensity falling upon a slab of thickness R immediately before the cavity, where R is some range, yet to be defined, of electrons produced by quanta of energy W.

Assuming $(dE/dx)_{\text{coll}}$ to be constant along the track of an electron, which is very nearly so in the energy region of interest, this average effect is given by

$$S(W)=\frac{1}{R}\int_{T-R}^{T} F(W)\tau(W)\,\mathrm{e}^{-\tau x}\,dx=\frac{1}{R}F(W)\,\mathrm{e}^{-\tau T}(\mathrm{e}^{\tau R}-1), \qquad \ldots\ldots(7)$$

which reduces to (6) in the limit of $R\rightarrow 0$.

We define S to be the *sensitivity*: it is the fraction of energy converted to ionization in first collision per unit thickness of wall at the depth T, per unit intensity incident upon the front wall of the chamber.

We have, however, to decide what range to use for R. R should clearly be, in consequence of the definition of S above, *the mean range in aluminium of the secondary electrons produced by quanta of energy W*. This quantity could in principle be determined numerically in terms of known cross sections, taking into account the bending of electron tracks by multiple collisions. Fortunately, however, it is known experimentally to sufficient accuracy for the present purpose, and is quoted by Fowler, Lauritsen and Lauritsen (1948). The curve of R as a function of W is reproduced in fig. 3, where we have extrapolated from 20 to 25 Mev (the curve is sufficiently linear to allow of this without appreciable error).

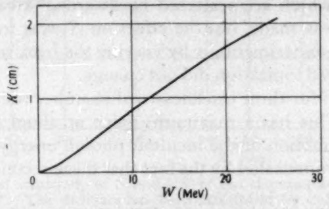

Fig. 3. Mean range in aluminium of secondary electrons produced by quanta of energy W.

3.3 *Second Collisions*

In this section we extend the methods of the previous sections to calculate the amount of ionization produced by those degraded quanta which result from one Compton collision in the undeflected beam.

Consider a photon which, after travelling a distance $x\,(<T)$ normally to the chamber surface without collision, suffers a Compton collision in a volume dr at x

and eventually reaches the cavity T by travelling a further distance r in the new direction at an angle θ to the normal. Take again unit incident intensity of energy W. The undeflected intensity at the depth x is then $I = \mathrm{e}^{-\tau x} = \mathrm{e}^{-\tau(T - r\mu)}$, where $\mu = \cos\theta$.

We may write the Klein–Nishina cross section in the form $\sigma_e(W, \mu)$ rather than $\sigma_e(W, E)$, since to each recoil energy E there corresponds a μ given by $[1 + W(1-\mu)]^{-1} = W'/W$, where $W' = W - E$ is the energy of the scattered quantum. Then the angular distribution of intensity is given by

$$\psi(\mu) = (W'/W)\sigma_e(W, \mu)$$
$$= \tfrac{1}{2} r_0^2 \left\{ \frac{1+\mu^2}{[1 + W(1-\mu)]^3} + \frac{W^2(1-\mu)^2}{[1 + W(1-\mu)]^4} \right\}, \qquad \ldots\ldots(8)$$

where r_0 is the classical electron radius (Heitler 1944, p. 156).

The contribution to the total intensity at r (i.e. at the surface of the cavity) in the direction of the incident beam, due to quanta scattered once from the volume dv at x containing NZ electrons per cm^3, is then $dI' = INZ\, dv[\mu\psi(\mu)/r^2]\, \mathrm{e}^{-\tau' r}$, where $\tau' = \tau(W')$ is the absorption coefficient for the degraded quanta of energy W'. The volume element is $dv = 2\pi r^2\, dr\, d\mu$, so that, integrating, we obtain

$$I' = 2\pi NZ\, \mathrm{e}^{-\tau T} \int_0^1 \frac{\psi(\mu)}{\omega(\mu)} [1 - \mathrm{e}^{-\omega T}]\, d\mu, \qquad \ldots\ldots(9)$$

where
$$\omega(\mu) = (\tau' - \tau\mu)/\mu. \qquad \ldots\ldots(9\,a)$$

We may now calculate the ionization produced at T in the same way as for the undeflected beam, except that we use the intensity I' given by (9) instead of unit intensity.

This leads to the relation

$$S'(W) = 2\pi NZ\, \mathrm{e}^{-\tau T} \int_0^1 \frac{\psi(\mu)}{\omega(\mu)} (1 - \mathrm{e}^{-\omega T}) \tau(W') F(W')\, d\mu. \qquad \ldots\ldots(10)$$

The function ψ is given by eqn. (8), and ω, defined by eqn. (9 *a*), is computed from the known absorption coefficients. The expression (10) does not include the effect of the finite electron range, since this is of negligible importance here owing to the lower energies involved in second scattering. Equation (9) does not include photons which are scattered backwards; a calculation of the back scattering, however, was made, but the effect on S' was found to be very small. This has been verified experimentally by varying the back wall of the chamber and noting that the measured ionization did not change.

The ratio of S' to S for three thicknesses of chamber wall, viz. 5, 7·5 and 10 cm, is shown in fig. 4. This has a maximum value at about 0·1 Mev. At energies below this, a greater fraction of the incident photon energy appears as secondary photons, but this is compensated by the fact that these secondary photons are more strongly absorbed.

In calculating the scattered intensity I' (eqn. (9)), we have taken into account only the normal component of the flux. Strictly, the integrand in eqn. (9) should be divided by μ. At high energies this approximation is good, since most of the secondary photons travel nearly in the forward direction ($\mu \simeq 1$). At energies below about 1 Mev, where more of the secondary photons travel at large angles, the omission of μ in the denominator of the integrand helps to compensate for the fact that in a practical chamber many of them pass out of the chamber wall before penetrating to a depth T.

The sensitivity corrected for second collision, and ignoring back scattering, is now $S_0(W) = S(W) + S'(W)$. This is shown in fig. 5. The scale has been multiplied by a suitable factor so that the curve gives a direct relation between current in the ion chamber and the number of photons falling on the front wall per cm² per sec (see § 3.5).

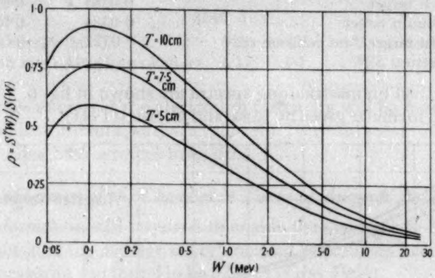

Fig. 4. Graph of S'/S, the ratio of the sensitivities due to the second-order and first-order beams.

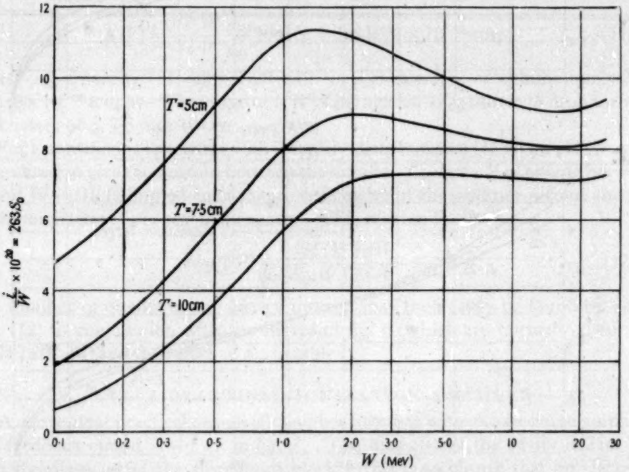

Fig. 5. Graph of the total sensitivity of $S_0 = S + S'$ of the chamber as a function of the incident quantum energy W. The ordinate has been multiplied by 263×10^{-20} so that the curve may be used directly to give $(1/W) \times$ (ionization current in amp/cm³ of cavity produced per quantum falling per second per cm² of the front wall of the chamber).

The sensitivity S_0 is a function of W, so that if a continuous spectrum is used an average value must be taken, given by

$$S_{\mathrm{av}} = \frac{\int \phi(W) S_0(W)\, dW}{\int \phi(W)\, dW},$$

where $\phi(W)$ is the intensity spectrum of the radiation.

Values of S_{av} calculated for the theoretical bremsstrahlung spectra from aluminium and tungsten targets for energies of 10, 15 and 25 Mev with a wall thickness of 5 cm are given in table 1.

Table 1

Peak energy of bremsstrahlung spectrum (Mev)	10	15	25
S_{av} for a tungsten target	0·0384	0·0378	0·0374
S_{av} for an aluminium target	0·0384	0·0378	0·0372
S_{av} for a tungsten target, first collision only (i.e. neglecting S')	0·0322	0·0324	0·0335

The theoretical bremsstrahlung spectra are shown in fig. 6. They have been computed from formulae given by Rossi and Greisen (1941).

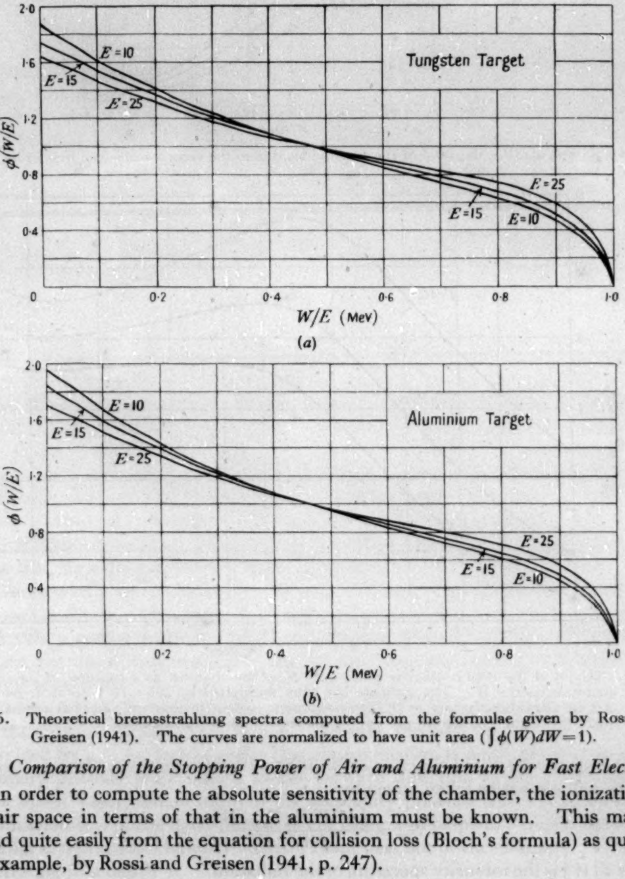

Fig. 6. Theoretical bremsstrahlung spectra computed from the formulae given by Rossi and Greisen (1941). The curves are normalized to have unit area ($\int \phi(W)dW=1$).

3.4. *Comparison of the Stopping Power of Air and Aluminium for Fast Electrons*

In order to compute the absolute sensitivity of the chamber, the ionization in the air space in terms of that in the aluminium must be known. This may be found quite easily from the equation for collision loss (Bloch's formula) as quoted, for example, by Rossi and Greisen (1941, p. 247).

The ionization loss is not independent of electron energy, though we have tacitly assumed that it is so in formulating the definition of S according to eqn. (7). The variation of the ratio of the ionization loss in air to that in aluminium does not, however, vary appreciably with energy, as the following table shows.

Table 2

Electron energy (Mev)	0·25	2	5	15	25
Ionization ratio Air/Aluminium $= r$	1·12	1·1	1·095	1·09	1·08

Now the average energy of the electron in the cavity will be much less than the energy of the incident photons, so that a value of 1·10 would seem to be a reasonable average. This value has therefore been used.

3.5. *Calibration of the Chamber in Terms of Amperes per Photon*

The only information still required to enable the chamber to be calibrated in amperes per photon is the average energy needed to produce one ion pair in air. This has been measured and found to be 32·0 ev (Gray 1944).

The ionization current per cm^3 of air space per quantum per cm^2 per sec may then be written as

$$i(W)=\frac{10^6\,W}{32\cdot0}\,\frac{\rho_{\rm air}}{\rho_{\rm al}}\,10\boldsymbol{e}rS_0=263\,WS_0\times10^{-20}\ \text{amp}, \qquad \ldots\ldots(11)$$

where $\rho_{\rm air}$ = density of air $=1\cdot29\times10^{-3}$, $\rho_{\rm al}$ = density of aluminium $=2\cdot7$, $\boldsymbol{e}=1\cdot6\times10^{-20}$ e.m.u. The curve of $i(W)/(W)$ against W is shown in fig. 5 for wall thicknesses of 5, 7·5 and 10 cm.

For a continuous spectrum with intensity distribution $\phi(W)$ eqn. (11) may be generalized to give the relation between the number of quanta N of energy between W and $W+dW$ falling on each square centimetre of the wall per second and the ionization current i per cm^3 of air space. This relation is

$$N=10^{20}\,\frac{i\phi(W)\,dW}{263S_{\rm av}W\int\phi(W)\,dW}. \qquad \ldots\ldots(12)$$

The number of quanta in any energy interval may then easily be found by using eqn. (12) in conjunction with the curves of fig. 6 (which are normalized so that $\int\phi(W)\,dW=1$) and the values of $S_{\rm av}$ in table 1.

§ 4. A PRACTICAL IONIZATION CHAMBER

A convenient practical design of chamber together with its associated amplifier and feedback circuit is shown in fig. 7. The diameter of the cavity is 2 in. less than the diameter of the aluminium block ; this is to ensure that no electrons which should pass through the cavity diffuse out of the edge of the block. The diameter of the cavity should be large compared with its thickness, otherwise many electrons will enter through its sides and the effective wall thickness of the chamber will be uncertain.

It has not yet been possible to calibrate the chamber with a known source. Nevertheless a number of measurements of ionization current against wall thickness have been taken for radiation from the synchrotron. A typical curve, taken at a peak energy of 23 Mev, is shown in fig. 8. The rise to a maximum and subsequent monotonic decrease may be seen. Theoretical points normalized in ordinate to give the best fit are also shown.

The agreement in the slope of the curve between theory and experiment at both 23 and 10 MeV is good. This is an indication that reasonable approximations have been made in the calculation, especially since the agreement is substantially worse if the second-order terms are neglected. In order to check that the chamber performance was not sensitive to exact geometry the depth of the cavity of fig. 7 was varied up to about 2 cm, and the thickness of the aluminium at the side of the cavity was reduced to 1 cm, but no measurable change in the curve was detected.

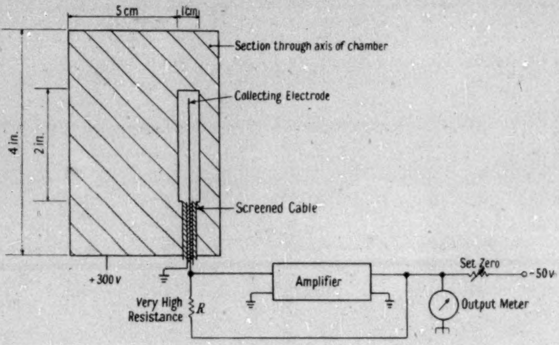

Fig. 7. Diagram of a practical ionization chamber, and circuit for measuring the current.

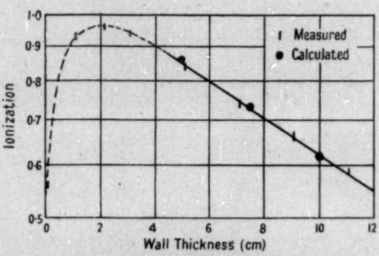

Fig. 8. Curve of ionization current against wall thickness obtained with 23 MeV bremsstrahlung from a tungsten target. Theoretical points normalized to give the best fit are also shown.

§ 5. CONCLUSION

The authors believe that the standard ion chamber described in this paper represents as accurate a monitor as can reasonably be devised with present knowledge and techniques for measuring the X-ray intensity from synchrotrons and betatrons with peak energies from about 10–25 MeV. Approximations have had to be introduced liberally to make the calculations manageable, but the error introduced thereby is probably not much in excess of the errors caused by uncertainties in the cross sections for the various processes. According to rough estimates based upon the accuracy of knowledge of cross sections etc., and upon the behaviour of S' at low energies, the calculation of sensitivity is expected to have a probable error of about 5% for X-ray energies above 5 MeV, and to be rather worse below this energy.

ACKNOWLEDGMENT

This work is published by kind permission of the Director, Atomic Energy Research Establishment, Harwell.

REFERENCES

Fowler, W. A., Lauritsen, C. C., and Lauritsen, T., 1948, *Rev. Mod. Phys.*, **20,** 236.
Gray, L. H., 1944, *Proc. Camb. Phil. Soc.*, **40,** 72.
Heitler, W., 1944, *Quantum Theory of Radiation*, 2nd edition (Oxford : University Press).
Mayneord, W. V., 1940, *Brit. J. Radiol.*, **13,** 235; 1950, *Ibid.*, Supplement No. 2, 125.
Mayneord, W. V., and Martin, J. H., 1950, *Brit. J. Radiol.*, Supplement No. 2, 212.
Rossi, B., and Greisen, K., 1941, *Rev. Mod. Phys.*, **13,** 240.

The Effect of Moisture on the Electrical Properties of Soil

By A. COWNIE and L. S. PALMER
Physics Department, University College of Hull

MS. received 13*th September* 1951

ABSTRACT. Measurements of the dielectric constant of soil containing different known percentages of moisture were made at a fixed frequency of 430 Mc/s. The method adopted involved the use of a coaxial transmission line terminated with a sample of the soil under test. The line consisted of a central rod with a concentric tube about 2½ metres in length. Measurements were made with soil samples containing from 4·1 % to 47·7% moisture. The dielectric constant was found to vary from 4·0 to 31·4. The values are shown graphically and compared with those obtained by nine other authors. The conductivity could not be measured accurately with the method used, but it was estimated to vary from about $1\cdot5\times10^{9}$ e.s.u. with 4% moisture to 4×10^{10} e.s.u. with 50% moisture.

§1. INTRODUCTION

During the past fifteen years at least nine authors have published measurements of the dielectric constant, electrical conductivity, etc., of various soils with different moisture contents for radio frequencies varying from 60 to 9 375 megacycles per second. In a few cases the percentage of moisture was measured; in other cases the soil was said to be either wet or dry. The recent measurements of dielectric constant that are relevant to the present work are shown graphically in fig. 1. The diversity of these results does not enable one to obtain a clear picture of the variation of the dielectric constant of soil either with moisture content or with frequency, whilst the different natures of the soils used by different experimenters introduce another variable, the effect of which cannot be taken into consideration when comparing the measurements on soils from different localities.

The main objective of the present work was to determine, at a fixed frequency of 430 Mc/s, the variation of the dielectric constant of a clay soil (upper boulder clay) for various known moisture contents. The hope that such measurement would be undertaken was expressed by Palmer and Forrester in 1941, when the war prevented the continuation of their work. The method they devised was based on an earlier publication by Palmer and Gillard (1938) on the current distribution in a long transmitting antenna. The method involved the measurement of the standing waves produced on such an antenna when it was

.B
5
2

actuated at one point and 'earthed' at the lower end in the soil under investigation. This method required a large quantity of soil and was, therefore, not suitable for experiments which necessitated a control of the moisture content.

§2. EXPERIMENTAL METHODS. APPARATUS AND PROCEDURE

(i) *Methods*

In order to overcome the above objection to the original antenna method, it was decided to replace the antenna by a coaxial transmission line provided with a detachable extension to contain a sample of the soil. This method is well known and has the advantage that only relatively small quantities of soil are required. Consequently, the moisture content was more readily controlled and measured. The thermojunction used in the original antenna method was replaced by an electric probe and crystal detector mounted on a carriage which could travel the length of the transmission line between the input and the soil termination, a modification which increased considerably the ease and speed with which the electrical measurements were made.

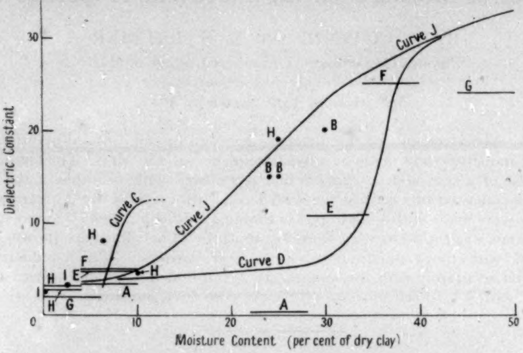

Fig. 1. Comparison of results (for key to lettering see below).

Reference	Author	Year	Mc/s
A	McPetrie	1934	200 (dry) 650 (wet)
B	Smith-Rose	1935	100
C	Banerjee and Joshi	1938	70·9
D	Chakravarty and Khastgir	1938	82
E	Palmer and Forrester	1941	407
F	McPetrie and Saxton	1945	60
G	Ford and Oliver	1946	3330
H	Straiton and Tolbert	1948	9375
I	Chatterjee	1950	450
J	Cownie and Palmer	1951	430

The method involves essentially the determination of the reflection coefficient of the end of that portion of the line which contains the soil. This coefficient may be deduced in the usual way from measurements of the standing wave ratio and from the position, relative to the air–soil boundary, of the standing waves set up on the line between the input and the termination.

Measurements were made on three different forms of termination to the line: (*a*) a length of soil sample sufficient to ensure complete absorption of the wave penetrating the air–soil boundary, (*b*) a short length of soil backed by a short-circuiting brass piston, and (*c*) the same arrangement as (*b*) but with the short-circuit a quarter of an air wavelength behind the soil. Although the constants of the soil could be determined from the reflection coefficients as measured by either of these methods, or more easily from the reflection coefficients of (*b*) and (*c*) together, it was found that the only satisfactory experimental method yielding consistent results was that employing termination (*b*) alone.

(ii) *Apparatus*

The coaxial line used in the above three methods was about $2\frac{1}{2}$ metres in length, with the outer tube of diameter 3·8 cm and the inner tube of diameter 0·95 cm. A slot of width 0·39 cm extended the whole length of the line. To the end of the outer conductor was fitted a sleeve into which an extension of the line, to contain the sample of soil, was screwed; the inner conductor likewise was fitted with a removable extension. The other end of the coaxial line was fitted with a sliding brass piston with provisions for clamping it to the inner and outer conductors to ensure good contact. A centimetre scale was inscribed on the outer conductor with the zero at an arbitrary point near the extremity of the line.

The high-frequency input was generated by a valve oscillator taken from a Type 33/L radar receiver which was modified so that its frequency was 430 Mc/s. The oscillator was loosely coupled to an input coaxial cable, the inner conductor of which was directly clamped to the axial rod of the transmission line. Measurements of the frequency of the oscillator were made with a crystal check wavemeter covering the range 85 to 1 000 Mc/s.

The detector circuit consisted of an electric probe feeding into a cartridge-type crystal detector connected through a high-loss coaxial cable to a Cambridge spot galvanometer. The circuit was tuned for maximum sensitivity by means of a small variable air condenser connected across a high-frequency choke between the inner and outer conductors to the crystal. The depth of penetration of the probe could be varied over a range of a few millimetres, and the probe was prevented from moving from its central position in the slot of the coaxial line. A short length of millimetre scale attached to the detector carriage lay along the centimetre scale engraved on the outer conductor.

(iii) *Procedure*

Preliminary experiments were carried out to check the frequency and power stability of the oscillator. These showed that the variation of the frequency over the range of power and load met with in the subsequent experiments was less than 0·05%. Observations of the detector galvanometer while the probe was stationary showed that the output of the oscillator after a period of ten minutes' operation was constant for all practical purposes. In order to provide a sensitive monitor for the measurements of power stability as the position of the probe was varied, a second probe was inserted in the coaxial line in the section remote from the soil sample. With a lossy soil termination in place there was no detectable change in the monitor galvanometer when the main detector probe was moved from a minimum to a maximum of the standing wave pattern.

The boulder clay on which measurements were made was obtained from a depth of about two feet beneath the field surface. Water was added to make the clay sufficiently soft to be forced through a fine mesh in order to remove particles of grit and fibre. The sample was allowed to dry as required. If the clay was still malleable it was worked to a homogeneous plastic state before it was packed into the tube. For clay so dry as to form a hard solid mass the sample was crushed to a fine powder and passed through a sieve before it was packed. The dry powdered clay was then poured into the sample tube closed at one end and pressed to a solid state with a heavy brass plunger. To pack the sample of wet clay, the clay was prepared in a homogeneous lump, free of air pockets, and the sample tube with its inner rod in place was forced through it so that it cut out and contained a length of a few centimetres of clay. This was then moved along the sample tube to the required position and pressed firm with the brass plunger. In this way it was hoped to eliminate air pockets and discontinuities in the sample.

The measurement of the reflection coefficient of the line termination was made by plotting the standing waves set up in the portion of the line between the input connection and the sample. The input carriage and the reflecting brass piston beyond it were set to give maximum galvanometer deflection before the experiment was begun. The modulus of the reflection coefficient was deduced from the maxima and minima of the standing waves, and the phase angle was determined from the distance of the nearest minimum from the face of the sample of clay.

Immediately after the electrical measurements, a sample of the clay was weighed and its moisture content measured. The weighed sample was heated in a silica ignition boat in a current of dry air, and the mass of water expelled was found from the increase in weight of two drying tubes containing calcium chloride.

§ 3. THEORETICAL CONSIDERATIONS

The general theory of concentric transmission lines is well known, and consequently only formulae directly applicable to the present methods need be considered.

The fundamental formula for the input impedance Z of a concentric transmission line containing a section of dielectric material of length l situated at a distance d from a perfectly conducting termination is given by

$$Z = Z_0' \frac{Z_0 \tanh \gamma d + Z_0' \tanh \gamma' l}{Z_0' + Z_0 \tanh \gamma d \tanh \gamma' l}, \qquad \ldots\ldots(1)$$

where Z_0' and Z_0 are the characteristic impedances of the line with and without the dielectric, and γ' and γ are the corresponding propagation constants. Let the complex reflection coefficient of the termination be $k(=(Z-Z_0)/(Z+Z_0))$, let k_0 denote the value of k for a very long line for which $Z=Z_0'$, and let $k=k_1$ when $d=0$ for which $Z=Z_0' \tanh \gamma' l$. Then for a very long line (i.e. l very large)

$$\frac{1-k_0}{1+k_0} = \frac{Z_0}{Z_0'} = \frac{\gamma'}{\gamma} \qquad \ldots\ldots(2)$$

and for a short-circuited line

$$\frac{1-k_1}{1+k_1} = \frac{Z_0}{Z_0' \tanh \gamma' l} = \frac{\gamma'}{\gamma} \coth \gamma' l. \qquad \ldots\ldots(3)$$

Since $\gamma'/\gamma = \sqrt{\bar{\epsilon}}$, where $\bar{\epsilon}$ is the complex dielectric constant, we have $(\gamma'/\gamma)^2 = \epsilon + j\epsilon'$, where ϵ and ϵ' are both real and refer respectively to the ordinary dielectric constant and to the lossy part arising from the conductivity of the material. From these considerations it is apparent that measurements of k_0 or of k_1 are sufficient to determine completely the complex dielectric constant of the sample of conducting dielectric.

Equation (2) is the theoretical basis for the experimental method using total absorption, whilst the method employing a short-circuited line is based on eqn. (3).

If K_0 and ϕ_0 are the modulus and amplitude of the reflection coefficient k_0, the values of ϵ and ϵ' may be written

$$\epsilon = \frac{(1-K_0^2)^2 - 4K_0^2 \sin^2 \phi_0}{(1+K_0^2+2K_0 \cos \phi_0)^2}, \qquad \epsilon' = \frac{4(1-K_0^2)K_0 \sin \phi_0}{(1+K_0^2+2K_0 \cos \phi_0)^2}.$$

In the case of the short-circuited line, eqn. (3) may be written $(1/\gamma l)(1+k_1)/(1-k_1) = (\tanh \gamma' l)/\gamma' l$ or, in terms of K_1 and ϕ_1,

$$\frac{(1+K_1^4 - 2K_1^2 \cos 2\phi_1)^{1/2}}{\beta_0 l(1+K_1^2 - 2K_1 \cos \phi_1)} \exp\left[j \tan^{-1} \frac{-(1-K_1^2)}{2K_1 \sin \phi_1}\right] = \frac{\tanh \gamma' l}{\gamma' l}, \quad \ldots\ldots(4)$$

where $j\beta_0 = \gamma$.

The left-hand side of this equation was found experimentally and $\gamma' l$ deduced from charts of the transcendental function on the right-hand side.

It is interesting to study the variation of the reflection coefficient k_1 as the length of sample varies. Such a study serves as a guide to the choice of sample lengths which will give convenient values of the measured moduli and amplitudes.

From eqn. (3), writing $\gamma' = \alpha + j\beta$,

$$k_1 = \frac{\sinh (\alpha+j\beta)l - (c/\omega)(j\alpha - \beta) \cosh (\alpha+j\beta)l}{\sinh (\alpha+j\beta)l + (c/\omega)(j\alpha - \beta) \cosh (\alpha+j\beta)l}.$$

Since $k_1 = K_1(\cos \phi_1 + j \sin \phi_1)$, the above gives

$$K_1 = \frac{\begin{array}{r}\{\frac{1}{4}[(c^2/\omega^2)(\alpha^2+\beta^2-\omega^2/c^2) \cosh 2\alpha l + (c^2/\omega^2)(\alpha^2+\beta^2+\omega^2/c^2) \cos 2\beta l]^2 \\ + (c^2/\omega^2)[\alpha \sinh 2\alpha l + \beta \sin 2\beta l]^2\}^{1/2}\end{array}}{\begin{array}{r}\frac{1}{2}[(c^2/\omega^2)(\alpha^2+\beta^2+\omega^2/c^2) \cosh 2\alpha l + (c^2/\omega^2)(\alpha^2+\beta^2-\omega^2/c^2) \cos 2\beta l] \\ - (c/\omega)[\alpha \sin 2\beta l - \beta \sinh 2\alpha l]\end{array}},$$

and

$$\tan \phi_1 = -\frac{2\omega}{c} \frac{\alpha \sinh 2\alpha l + \beta \sin 2\beta l}{(\alpha^2+\beta^2-\omega^2/c^2) \cosh 2\alpha l + (\alpha^2+\beta^2+\omega^2/c^2) \cos 2\beta l}.$$

In fig. 2 the variations in K_1 and ϕ_1 are plotted against the length of sample for a medium of dielectric constant 20 and loss angle $\delta = \tan^{-1}\frac{1}{2}$.

In a similar way it may be shown that the graphs of K_2 and ϕ_2 represent the variations of these quantities with length of soil sample when the short-circuiting plate is moved back a quarter of an air wavelength from the sample.

§ 4. RESULTS AND DISCUSSION

The 19 results obtained by the short-circuit method (eqn. (4)) are shown graphically in fig. 3. This graph is reproduced in fig. 1 (curve J) in order to facilitate comparison with the results published by other authors. The fact that the graph has a point of inflection cannot be explained by any simple theory pertaining to mixtures of soil particles and water. On the other hand, if the moisture below about 15 or 20% behaves like the so-called 'bound' water with an effective dielectric constant of the order of that of ice, and above 20% acts as 'free' water with its normal value of dielectric constant, then a curve of the form obtained experimentally can be explained, at least qualitatively. It is proposed to pursue this point of view quantitatively.

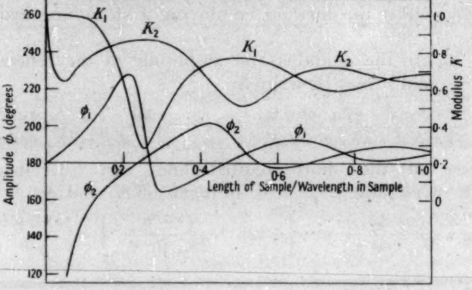

Fig. 2. Variation of amplitude and modulus of reflection coefficients with sample length.

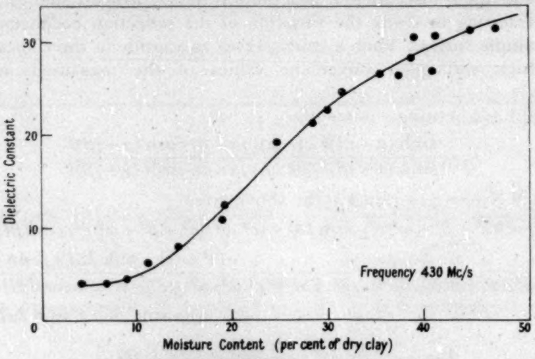

Fig. 3. Variation of dielectric constant with moisture content.

Methods using other forms of line termination were found to give less reliable results, and are therefore not reproduced in fig. 3. However, 63 other measurements were made before the short-circuit method was finally adopted, and these gave values of the dielectric constant not inconsistent with those shown.

A source of appreciable error was thought to lie in the measurement of the length of the sample, which could not be made to a greater accuracy than to the nearest half millimetre, but calculations with typical experimental values showed that an error of 0·5 mm in 4 cm of wet clay or in 10 cm of dry clay produced an error no greater than 1% in the dielectric constant of the clay.

The accuracy of measurement of the reflection modulus K depended on several factors, principally the accuracy of the galvanometer readings and the behaviour of the detector crystal. It was concluded that over the range in which the crystal obeyed a square law to within a few per cent the measurements of K were accurate to within 4%. The phase angle ϕ of the reflection coefficient could be measured to the nearest half degree, corresponding to location of the minimum of the standing wave pattern to the nearest half millimetre. The estimated probable error in the dielectric constant arising from these experimental errors varied from 5% for wet samples to 3% for dry samples, giving an overall accuracy of within some 6% to 4%.

The values of the dielectric loss obtained by the short-circuit method were subject to larger errors. Consequently it was only possible to make a rough estimate of the variation in the conductivity of the soil with changes in its moisture content. This estimate leads to the conclusion that the conductivity increases from about $1{\cdot}5 \times 10^{9}$ e.s.u. with 4% moisture to about 4×10^{10} e.s.u. with 50% moisture. These results, although they agree with the values obtained by a few authorities, are not thought to be sufficiently accurate to justify serious comparison with those obtained by more precise methods.

REFERENCES

Banerjee, S. S., and Joshi, R. D., 1938, *Phil. Mag.*, **25,** 1025.

Chakravarty, M. K., and Khastgir, S. R., 1938, *Phil. Mag.*, **25,** 795.

Chatterjee, S. K., 1950, *Indian J. Phys.*, **24,** 143.

Ford, L. H., and Oliver, R., 1946, *Proc. Phys. Soc.*, **58,** 265.

McPetrie, J. S., 1934, *Proc. Phys. Soc.*, **46,** 637.

McPetrie, J. S., and Saxton, J. A., 1945, *J. Instn. Elect. Engrs.*, **92,** Pt. III, 256.

Palmer, L. S., and Forrester, G. R., 1941, *Proc. Phys. Soc.*, **53,** 479.

Palmer, L. S., and Gillard, K. G., 1938, *J. Instn. Elect. Engrs.*, **83,** 415.

Smith-Rose, R. L., 1935, *Proc. Phys. Soc.*, **47,** 923.

Smith-Rose, R. L., and McPetrie, J. S., 1934, *Proc. Phys. Soc.*, **46,** 649.

Straiton, A. W., and Tolbert, C. W., 1948, *J. Franklin Inst.*, **246,** 13.

LETTERS TO THE EDITOR

The Electric Breakdown of Alkali Halide Crystals

Reliable experimental data about the intrinsic strength of alkali halide crystals would be of value in testing the available theories of breakdown in solids. A number of workers (Austen and Whitehead 1940, Hippel and Alger 1949, Malmlöw 1943) have made measurements, but disagreement exists between the various sets of published results, and it cannot yet be said that data of sufficient accuracy are available.

When a number of apparently similar specimens were tested under the same conditions, previous workers observed considerable scatter in the values obtained for the breakdown strengths. This might indicate the use of imperfect experimental techniques, but in the case of the more recent work the conclusion is hardly likely because considerable improvements have taken place during the last few years. In the course of measurements recently made by ourselves we also have observed scatter. For reasons given below we consider that its principal cause was inherent in the specimens themselves, and was not due to extraneous effects.

The measurements were made with d.c. voltages applied to specimens of KCl and NaCl prepared from single crystals grown by the method of Kyropoulus. The test specimens were recessed and the electrode system was similar to that developed and recommended by the Electrical Research Association (Whitehead 1951). The specimens were highly polished and care was taken to eliminate those with small incipient cracks and surface

.B
5
2

scratches in the vicinity of the bottom of the recess. The electrodes were of colloidal graphite, or of silver which was deposited by evaporation in a vacuum, and the immersion medium was either transformer oil, toluene or pentane.

The scatter was found to be independent of both the immersion medium and the electrode material, and when the results were examined of more than 100 breakdown measurements made on specimens of thickness between 0·004 in. and 0·02 in. no correlation could be obtained between sample thickness and intrinsic electric strength. These facts suggest that spurious discharges in the immersion medium and other extraneous effects were absent from the measurements, and that scatter was therefore a property of the specimens used. This conclusion is borne out by the result of the experiment illustrated by fig. 1.

Figure 1 (*a*) is a histogram of 30 independent measurements made at room temperature on specimens of KCl. The breakdown strength exhibited considerable scatter. Figure 1 (*b*) is a histogram of 30 measurements, made under conditions identical with those in the previous measurements, on specimens prepared from the same parent crystal. The only known difference between the two sets of specimens is that those of fig. 1 (*b*) had been annealed, before applying the graphite electrodes, by slowly cooling them from a temperature just below the melting point, whereas the specimens of fig. 1 (*a*) had not been annealed. Annealing the crystals had appreciably reduced the scatter, mainly by eliminating the high breakdown values.

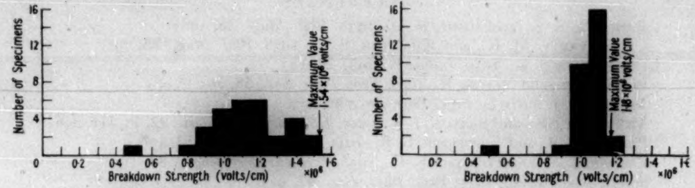

(*a*) Unannealed specimens at 20°c. (*b*) Annealed specimens at 20°c.

Fig. 1. Effect of annealing KCl crystals on breakdown strength.

A possible explanation of the effect is that annealing had produced a more uniform batch of specimens by relieving strains which may have been set up during the growth of the parent crystal, or during the preparation of the test specimens. Evidence in favour of this was obtained by viewing through a strain analyser a number of specimens prior to breakdown. Many of the unannealed specimens exhibited considerable strain and subsequently were found to possess high values of electric strength, but the annealed specimens were considerably less strained and the batch was much more uniform.

It therefore appears that scatter in measured values of the intrinsic electric strength of ionic crystals may possibly indicate the use of strained crystals, and in this event the practice of selecting as the true value the maximum of a number of measurements is not justified. It seems that some of the earlier work on alkali halide crystals may have been carried out in this way and, unfortunately, previous workers have seldom given details of any thermal treatment which may have been applied to their specimens.

The authors wish to thank Professor Kearton, Mechanical Engineering Department, University of Liverpool, who kindly placed a strain analyser at their disposal, and Mr. Stevenson of Aberdeen University, who assisted by supplying a large crystal.

The work has been carried out in Electronics Department, University of Liverpool.

The University,
Liverpool.
22nd January 1952.

J. H. Calderwood.
R. Cooper.
A. A. Wallace.

Austen, A. E. W., and Whitehead, S., 1940, *Proc. Roy. Soc.* A, **176**, 33.
von Hippel, A., and Alger, R. S., 1949, *Phys. Rev.*, **76**, 127.
Malmlöw, G., 1943, *Ark. Mat. Astr. Fys.*, **30B**, 1.
Whitehead, S., 1951, *Dielectric Breakdown of Solids* (Oxford : Clarendon Press), pp. 9–11.

Positive Current Creep in Selenium Rectifiers

When a constant reverse voltage is applied to a selenium rectifier, the current is not constant, but varies with time. The phenomenon is called current creep, and increase in current with time constitutes positive creep. Henisch and Ewels (1950) have proposed that positive creep is due to the power dissipation in the barrier layer. We have recently carried out the following experiments, which indicate that this explanation may not always be valid.

Henisch and Ewels found that the temperature of the rectifier used in their experiments increased in a manner consistent with the observed positive creep. But since they ensured the dissipation of considerable power in the barrier layer by passing current of up to about 100 mA, it seemed desirable to repeat the experiment under conditions less favourable to the thermal theory. The results of such an experiment, carried out at about 20°c on a commercial selenium rectifier, are illustrated by the figure.

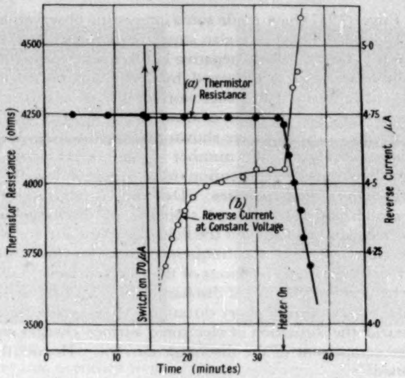

Positive creep in a selenium rectifier at 20°c.

Curve (*a*) shows the observed variation in the resistance of a thermistor attached to the counter electrode of the rectifier. A preliminary experiment had shown that the resistance of this device decreased by 100 ohms when its temperature was raised from room temperature by 1°c. The thermistor was connected in a bridge circuit that enabled a change in temperature to be measured of about $\frac{1}{500}$ °c. The rectifier was mounted in a draught-proof box and, when the rate of change of temperature had become small, a reverse current of 170 μA was passed through it. After one minute the current was suddenly reduced to about 4·1 μA. The ensuing positive creep is illustrated by curve (*b*). During the 17-minute period of positive creep no significant change occurred in the temperature of the rectifier (curve (*a*)). At the end of this period a small heater mounted underneath the base electrode was switched on. Instantly the current (at constant voltage) increased, and the resistance of the thermistor decreased. However, the temperature rise required to cause a change in current equal to that observed during the period of current creep was many times greater than the change in temperature which occurred during current creep. Thus, whilst high power dissipation may be a factor which favours positive creep, the present experiments have shown that it is not an essential condition, and some other mechanism of positive creep must have been simultaneously operative.

This possibility is supported by the following experimental fact. We have found, as Williams and Thompson (1941) have indicated, that positive creep often occurs when the applied reverse voltage is suddenly reduced. This effect has been observed at 20°c, when the temperature coefficient ($\delta I/\delta T$ at constant voltage) was positive, and at -74°c when it was negative. Positive creep due to thermal effect may have occurred at −74°C, but was very unlikely at 20°C because the power dissipation was reduced when the current decreased.

We wish to thank Messrs. Standard Telephones and Cables Ltd., who have kindly supplied a number of rectifiers, and Mr. E. A. Richards of that company for his interest in the work.

Department of Electrical Engineering : Electronics,
The University, Liverpool.
30th January 1952.

R. Cooper.
J. Harrington.

Henisch, H. K., and Ewels, J., 1950, *Proc. Phys. Soc.* B, **63**, 861.
Williams, A. L., and Thompson, L. E., 1941, *J. Instn. Elect. Engrs.*, **88**, Pt. I, 353.

The Mechanism of the Low-Frequency Electrodeless Discharge in Chlorine and the Influence of Irradiation

Harries and von Engel (1951) have made some interesting observations on silent electrical discharge through chlorine. They have also suggested a theory of the discharge and have offered an explanation of the so-called ‘ negative light-effect’, consisting of a diminution of discharge current on irradiation as observed by Joshi and his co-workers (Joshi 1943, Joshi and Deo 1944). It appears that earlier work on the same subject by Deb and Ghosh (1946, 1948 a, b) has escaped the attention of these authors. Deb and Ghosh have studied the discharge in an ozonizer tube and have shown that the discharge current is of a complex nature formed by the superposition of a number of component currents of different types. Amongst these they drew particular attention to a series of low-frequency pulses and a larger number of very high frequency pulses. Deb and Ghosh traced the origin of the low-frequency pulses to alternate starting and stopping of discharge under the combined influence of the externally applied field and the field due to the surface charges formed on the electrodes (inner glass walls). The high-frequency pulses were ascribed to the discharge of the surface charges from the different regions of the electrode surfaces. These conclusions were supported by the observed nature of discharge current in an ozonizer tube excited by unidirectional voltage pulses of very short duration. It was also shown that the effect of irradiation was to restrict the formation of electronic surface charges and thus to reduce the high-frequency pulse component of the discharge current. Hence, the observed negative light effect is explained.

The mechanism of discharge suggested by Harries and von Engel closely follows that of Deb and Ghosh, except that they do not distinguish between the high-frequency and low-frequency types of pulses. They trace the origin of the negative light effect to a different cause, namely, photodissociation of chlorine molecules near the electrode surface. The correctness of this viewpoint depends on whether or not there exists a threshold wavelength at 4800 A corresponding to the dissociation energy of chlorine. Some observations by Joshi (1945) on chlorine with a sodium lamp seem to contradict its existence. In this connection, it may be interesting to mention that the possible formation of an absorbed surface layer on the glass electrodes (as distinct from the “ boundary layer consisting of ions and excited molecules ”, as suggested by Joshi) was also pointed out by Deb and Ghosh.

Quite recently we have extended Deb and Ghosh's hypothesis further and have shown that it is possible not only to explain the details of the more common ‘ negative ’ effect but also the ‘ positive ’ effect (viz. an increase of discharge current on irradiation) which is sometimes observed at high pressure and low applied voltages. Details of our work will be published very soon.

Institute of Radiophysics and Electronics,
University of Calcutta.
8th January 1952.

A. K. Saha.
M. Ghosh.

Deb, S., and Ghosh, N., 1946, *Science and Culture Calcutta*, **12**, 17; 1948 a, *Ibid.*, **14**, 39 ; 1948 b, *J. Indian Chem. Soc.*, **25**, 449.
Harries, W. L., and von Engel, A., *Proc. Phys. Soc.* B, **64**, 916.
Joshi, S. S., 1943, *Proc. Indian Sci. Cong.*, Part II, 74 ; 1945, *Current Science*, **14**, 175.
Joshi, S. S. and Deo, P. G., 1944, *Nature, Lond.*, **153**, 434.

Austenite in Low Carbon Iron

In the course of work on the quench-ageing of ingot iron ($C=0\cdot026\%$) we have examined the grain boundaries by electron diffraction. In the reflection method the diffraction pattern arises by transmission through surface asperities. As has also been reported by other workers (Trotter *et al.* 1949), we have found that when a specimen previously quenched from 700°c is polished and etched with nital, the grain boundaries are raised above the general level of the surface. The grain boundaries are thus possible diffracting regions.

Examination of such a specimen shows a few spots corresponding to α-iron together with strong slightly diffuse continuous rings corresponding to a face-centred cubic structure with $a_0=3\cdot63\pm0\cdot01$ Å (fig. 1). This is the lattice parameter of an austenite. (The three strongest reflections of the air-formed oxide are also visible as diffuse rings.)

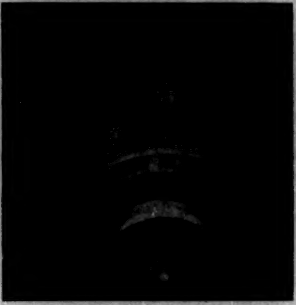

Fig. 1. Electron diffraction reflection pattern of ingot iron quenched from 700°c, polished and etched.

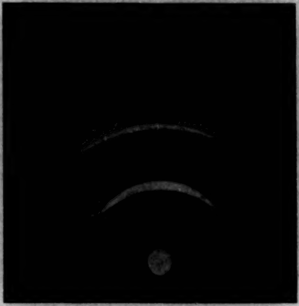

Fig. 2. Same specimen abraded on 000 emery.

The actual lattice spacing of austenite depends upon the amount of carbon in interstitial solid solution. The measured values range from 3·56 Å with no carbon to 3·64 Å with 1·7% weight of carbon, the limit of solid solubility. In view of the error in measurement of the radii in the diffraction photograph the carbon content of the austenite found in the quenched specimen could range from 0·85 to 1·7%. Hence the pattern must arise from an austenite with high carbon content.

The slight diffuseness of the austenite rings suggests that the particle size is very small and the lattice possibly distorted.

It has been confirmed that the austenite is confined to the grain boundaries by examining a specimen abraded on 000 emery. Here asperities are produced uniformly over the whole surface of the specimen. The pattern consists only of sharp continuous ferrite rings, showing that the bulk of the material is certainly body-centred cubic ferrite (fig. 2). We have also examined a specimen which had been furnace cooled from 700°c, polished and etched. This again showed only ferrite rings.

Thus it appears that austenite may be formed as a grain boundary film during quenching and retained with ferrite at room temperature. Hitherto retained austenite has been observed only after quenching from temperatures above the α–γ transformation temperature in steels containing a much greater proportion of carbon.

Various theories have been advanced to account for the yield phenomena in iron and a recent explanation by Hall (1951) requires the existence of a grain boundary film differing in composition from the bulk material. It has been known for some time that under suitable conditions of heat treatment, cementite can form as grain boundary films in iron; it may be that austenite films are also effective in influencing the mechanical properties.

Laboratory for the Physics and Chemistry of Surfaces,
Department of Physical Chemistry,
University of Cambridge.
J. W. Menter.

Department of Metallurgy,
University of Cambridge.
J. Nutting.
A. L. Tsou.

12th February 1952.

Hall, E. O., 1951, *Proc. Phys. Soc.* B, **64**, 747.
Trotter, J., McClean, D., and Clews, C. J. B., 1949, *Electron Microscopy*, Institute of Metals Symposium (London : Institute of Metals), p. 75.

Report of the Copenhagen Meeting of the General Assembly of the International Union of Pure and Applied Physics

The General Assembly of the Union met at Copenhagen on the 11th, 12th and 13th July 1951 on the occasion of a conference organized by Professors N. Bohr and S. Rozental under the auspices of the Union.

The Assembly sent a message to the Director-General of UNESCO expressing its gratitude for the very effective help which that organization extends to the Union. The Assembly also expressed its gratitude to all members of the former Executive Committee, to such Vice-Presidents as are not eligible for re-election and in particular to the President, Professor H. A. Kramers.

The following elections were made unanimously :

Executive Committee

President : N. F. Mott (Bristol).

Vice-Presidents : E. Amaldi (Rome), G. Borelius (Stockholm), A. Heyrowsky (Prague), P. Huber (Bâle), K. S. Krishnan (New Delhi), M. L. Oliphant (Canberra), J. C. Slater (Cambridge, Mass.), and J. A. Wheeler (Princeton, N.J.).

Secretary-General : P. Fleury (Paris).

Specialized Committees

1. *Finance* : E. Bauer (Paris), C. J. Gorter (Leiden).
2. *Symbols, Units and Nomenclature* : A. Pérard, President (until the end of 1951), H. König, President (Berne), J. de Boer, Secretary (Amsterdam), J. Cabannes (Paris), E. Guggenheim (Reading), E. Perucca (Turin), J. H. Van Vleck (Cambridge, Mass.).
3. *Thermodynamics and Statistical Mechanics* : J. Mayer, President (Chicago), I. Prigogine, Secretary (Brussels), E. Bauer (Paris), J. A. Beattie (Cambridge, Mass.), S. R. de Groot (Utrecht), E. Rushbrooke (Newcastle, U.K.).
4. *Cosmic Rays* : P. M. S. Blackett, President (Manchester), L. Leprince-Ringuet, Secretary (Paris), C. D. Anderson (Pasadena, California), G. Bernardini (Rome), H. J. Bhabha (Bombay), M. S. Vallarta (Mexico).
5. *Very Low Temperatures* : F. E. Simon, President (Oxford), C. J. Gorter, Secretary (Leiden), F. C. Brickwedde (Washington, D.C.), K. Clusius (Zürich), A. van Itterbeek (Louvain), C. E. Lane (Newhaven, Conn.).
6. *Publications* : J. H. Awbery, President (London), G. A. Boutry, Secretary (Paris), M. Fierz (Bâle), A. D. Fokker (Amsterdam), E. Hutchisson (Cleveland, Ohio), E. Perucca (Turin).
7. In addition the General Assembly has decided to form a new specialized committee for *Acoustics*. It has named the following to join in this Committee :

R. H. Bolt, President (Cambridge, Mass.), C. W. Kosten, Secretary (Delft), F. Canac (Marseille), F. Ingerslev (Copenhagen), A. Giacomini (Rome), E. Mayer (Göttingen), W. P. Wilson (Tadworth, U.K.).

Mr. Wilson having been unable to accept, his name was replaced by that of Mr. W. West (London).

The following proposed conferences were discussed and were considered favourably, though it was agreed that the list was provisional, and could be changed by the Executive Committee according to the funds available and in consequence of suggestions of local organizing Committees.

1952. Structure and properties of solid surfaces (Chicago: September or October 1952).
Spectroscopy of β and γ rays (Amsterdam: the dates were fixed later as 1st–7th September 1952).
Thermodynamics of phase transitions (Paris: the dates were fixed later as 3rd–7th June 1952).
The relation between optics and the study of short waves, or some other subject in optics (Milan in April or May 1952).
1953, Nuclear physics (Italy).
1954. Physiological optics and its connection with instrumental optics (Spain ?).
Fundamental problems of theoretical physics (Kyoto).
Thin films (Bristol).
Acoustics (at a place to be fixed).
Spectroscopy (at a place to be fixed).

The various specialized Committees reported on their work. The summary printed here includes only the report of the Committee for Symbols, Units and Nomenclature (S.U.N.), which was adopted by the General Assembly. Their recommendations are as follows:

1. It was recommended that the use of the word 'billion' should be avoided in scientific literature. The use was recommended, for example, of either 10^9 ev or Gev (as agreed by IUPAP in 1948).

2. After prolonged discussion, the S.U.N. Committee decided, so as not to take any steps which would increase the cost of printing, that the recommendations adopted in 1948 concerning the indices affixed to the symbols for the chemical elements should not be changed.

3. IUPAP recommended to physicists who wish to confine the word 'isotope' to different atoms having the same atomic number, the use of the word 'nuclide' to describe atoms which are identical both as regards their atomic number and their mass number. This recommendation is only to take effect after agreement with the Union of Chemistry.

4. The practical system of units, which will be called the Giorgi system or the m.k.s.a. system, is to be based on the following units: metre, kilogram-mass, second, ampere; in certain cases a different choice of four independent units could be made.

5. Since, in the near future, the c.g.s. system and the m.k.s.a. system may both be employed at the same time in pure and applied physics, and in order to facilitate the conversion of one of these units into the other, the introduction is recommended, with a view to defining the secondary units, of the following c.g.s. systems founded on the *four* principal units: (*a*) the c.g.s. electrostatic system, or c.g.s.e. system, based on the centimetre, the gramme, the second and the electrostatic unit of charge; (*b*) the electromagnetic c.g.s. system, or c.g.s.m. system, based on the centimetre, the gramme, the second and the deca-ampere.

6. (*a*) It was recommended that IUPAP suggest to the International Commission of Electrotechnics that a joint Committee should be set up to formulate recommendations on all questions concerning rationalization of units. (*b*) It is not desirable to recommend to physicists that only rationalized equations should be used or only non-rationalized equations. (*c*) The General Assembly of the Union of Physics considers that, in the case of rationalized equations, the rationalization should be obtained by the introduction of new measures.

7. The International Union of Physics authorizes the publication of the list of symbols of which the adoption is recommended by the S.U.N. Committee.

.B
5
2

REVIEWS OF BOOKS

Industrial High Vacuum, by J. R. Davy. Pp. viii + 243. (London: Pitman, 1951.) 25*s*.

Many years of practice in industrial applications of high vacuum technique form the solid basis of this book, and many observations and practical hints from the author's experience will be of great value to the reader. On the whole the author confines himself to his own experience. This is a limitation which may well be excused in view of the wide field covered, but it leads to numerous statements, often made in a very dogmatic form, which will not be accepted by others. The author appears, for example, to have had bad experiences with mercury diffusion pumps, and the sentence on p. 13, " mercury pumps are unsatisfactory for most evaporation processes, particularly the formation of aluminium films ", will come as a surprise to many.

Much useful information is contained in the first twelve chapters, dealing with vacuum technique in general, though there is no mention of the powerful and well-known method of using hydrogen in connection with a Pirani gauge for detection of small leaks.

The remainder of the book deals mainly with molecular distillation, deposition of thin films of metals and dielectrics, vacuum metallurgy and vacuum hydration. Even those who are familiar with these subjects will find many valuable hints.

Throughout the book the excursions into other fields, including history and poetry, are rather numerous. A sentence such as (p. 130) " The immense power locked in the atom, demonstrated to the world with spectacular finality as part of the barbarity of war, still remains incomprehensible to the layman, though the calculation is very simple " does not really help in the understanding of kinetic theory; and poetical effusions such as, on p. 162, " The soundless flicker of the discharge, so innocent in its pastel shades of heliotrope and blue, so lethal in its serried salvoes, scorching the dross off the surface of the glass . . . ." have been too liberally dispensed.

These are mere oddities; but unfortunately the theoretical interpretations of observed phenomena are frequently handled in the same fanciful way, such as the attempt to explain the cleaning effect of a discharge (p. 79) and the section headed The Theory of Molecular Packing (pp. 131–137). " In the evaporation process, molecules are allowed to evaporate in clusters of any size up to visible particles and to combine in flight " (in a high vacuum evaporation !).

It is unfortunate that throughout the book the theoretical jargon makes it difficult to disentangle observed facts from interpretations and generalizations. Many readers will be interested in the facts, few in the theoretical views of the author.

H. KUHN.

Mathematical Engineering Analysis, by Rufus Oldenburger. Pp. xiv + 426. (New York and London: Macmillan, 1951.) 45*s*.

According to the preface, the purpose of this book is to train the industrial research man to set up physical problems, amenable to mathematical treatment, in a form that can be conveniently handled by mathematical methods, and it is based on lecture courses which were given by the author in two American institutions. It " is intended to serve as a text in courses on engineering analysis and industrial physics and as a reference work for research directors in industry, for engineering analysts, for development engineers, and for applied scientists in various fields of learning ". The following branches of Physics are discussed: Mechanics of Rigid Bodies (65 pp.); Electricity (108 pp.); Heat (89 pp.); Elasticity (61 pp.); Fluid Mechanics (53 pp.).

There can be no doubt as to the excellence and the urgency of the purpose underlying this book, but whether the author has succeeded in fulfilling his aim is another matter. It is presumably inevitable that there should be great variation in standard in a book addressed to such a wide circle of readers; at the same time, this consideration scarcely justifies the inclusion of treatments which border on the ingenuous, e.g. the explanation of the action of a triode on p. 133 and such statements as " the density of an elastic member should be taken constant unless it is decidedly otherwise " (p. 334). It is also difficult to see why it should be thought necessary to include photographs for example, of " a group of industrial resistors ", of " a midget industrial condenser " and of " a collection of industrial triodes " in a book which treats quite advanced topics.

To a British physicist, this lack of uniformity and homogeneity is the worst feature of the book and it detracts from its value; this is a pity, because the author has certainly succeeded in collecting a large number of interesting problems of the type likely to arise in day-to-day industrial research and he derives and discusses the equations governing the phenomena in lucid fashion. If the author were to prune his text ruthlessly, rejecting those portions which are naïve and irrelevant, there would remain a book which would be an invaluable guide to many young physicists starting their industrial careers on this side of the Atlantic.

R. M. D.

Differential Equations, by H. B. PHILLIPS. Pp. viii + 149. 3rd Edition, revised. (New York: Wiley and Sons; London: Chapman and Hall, 1951.) 24*s*.

This is a most attractive introduction to the subject, intended mainly for physicists and engineers. While providing some formal instruction in the solution of simple ordinary differential equations, most emphasis is placed on the setting-up and solution of differential equations arising in Applied Mathematics, Physics, Chemistry, etc., such physical principles as are required being briefly described in the text.

.B
5
2

Chapter I deals with those first-order equations which can be solved by separation of the variables, with a wide variety of applications.

Chapter II completes the work on first-order equations, exact, linear and homogeneous equations being discussed. The integrating factor for the general linear equation is merely stated and verified. A direct derivation would take very little extra space. The alternative method of solving the same type of equation given on p. 44 so obviously comes to the same thing that it could well be omitted. The chapter ends with a brief description of simultaneous equations and solution by change of variable.

The simpler types of second-order equation, i.e. those in which x or y is explicitly absent and homogeneous equations, are dealt with in Chapter III. Theoretical discussion is confined to eight pages only, but there are many worked examples, including a section on the motion of dynamical systems of varying mass.

The final chapter treats linear equations of the nth order with constant coefficients in an elementary way, operational methods receiving only a brief mention.

In addition to about seventy illustrative examples worked out in full in the text, there are nearly five hundred exercises, for which answers are provided at the end of the book.

A. N. GORDON.

Jets gazeux sensibles aux sons et aux ultra-sons, by M. DUBOIS. Pp. 65. (Paris: Ministère de l'Air, 1951.) No price given.

The sensitive flame is mostly known in this country of late years from Andrade's Guthrie Lecture of 1941 and the work of G. B. Brown. In France jets in general have been a fairly common subject of research in the past ten years and that not so much for their industrial interest as on a purely academic level.

Dr. Dubois has made a careful and exhaustive study of the behaviour of sensitive jets in experiments particularly at high frequencies but cannot be said to have added much to our knowledge of the causes of their behaviour, which without taking elaborate precautions is too erratic to justify their use as quantitative detectors of sound or ultrasonics.

E. G. R.

CONTENTS FOR SECTION A

PAGE

Mr. P. R. Tunnicliffe and Mr. A. G. Ward. The Relative Ionization Produced by Low Energy Protons, Deuterons and Alpha-Particles in Various Gases . 233

Dr. R. Latham and Dr. J. M. Cassels. The Inelastic Scattering of Very Slow Neutrons by Iron 241

Dr. H. Messel and Prof. H. S. Green. The Angular Distribution of Scattered Nucleons in High Energy Nuclear Collisions 245

Dr. F. M. Kelly. The Nuclear Magnetic Moment of ${}^{197}_{79}$Au 250

Dr. F. D. S. Butement. A Radioactive Isomer of ^{166}Ho 254

Mr. I. D. Campbell and Dr. J. R. Prescott. The Structure of Extensive Showers 258

Mr. W. R. S. Garton. Investigations of Atomic and Molecular Absorption Spectra : I—General Features. II—Schumann Region Absorption Spectrum of Gallium Vapour 268

Mr. G. Drummond and Dr. R. F. Barrow. The Ultra-Violet Absorption Spectra of GeO, GeS, GeSe and GeTe 277

Letters to the Editor :

Mr. R. Cade : Mr. W. B. Smith-White. On Mechanical Action in Dielectrics 287

Dr. J. H. E. Griffiths and Mr. J. A. Powell. Anomalous Dielectric Loss in some of the Alums 289

Dr. Mary P. Lord. Further Evidence for the Lord–Rees–Wise Theory of Luminescence Decay of ZnS.Ag 291

Dr. R. I. Garrod. The Use of Gold Leaf as a Reference Material in the Determination of Lattice Constants by Electron Diffraction . . . 292

Prof. E. A. Owen. The Crystal Parameters of Beryllium 294

Mr. R. A. Allen, Dr. L. E. Beghian and Mr. J. M. Calvert. Response of Organic Scintillators to d–d Neutrons 295

Mr. A. Ashmore and Dr. J. F. Raffle. New Energy Level in ^{7}Li . . 296

Mr. D. L. Livesey and Dr. C. L. Smith. The Photo-disintegration of Nitrogen-14 Nuclei 297

Mr. M. R. Padhye and Mr. S. R. Desai. Long Wavelength Absorption Band of Thiophene 298

Report of the Copenhagen Meeting of the General Assembly of the International Union of Pure and Applied Physics 299

Reviews of Books 301

Contents for Section B 302

Abstracts for Section B 303

ABSTRACTS FOR SECTION A

The Relative Ionization Produced by Low Energy Protons, Deuterons and Alpha Particles in Various Gases, by P. R. TUNNICLIFFE and A. G. WARD.

ABSTRACT. Mono-energetic neutrons have been used to produce recoil protons, deuterons and α-particles in a proportional counter. The maximum pulse sizes produced by the different recoil particles are compared with the accurately known ratios of maximum recoil energies. From the results for protons and deuterons it can be inferred that, for protons between 200 and 550 kev energy, the ionization is proportional to the energy with a deviation of less than 1%. The total ionization in argon produced by a proton is about 8% greater than that of an α-particle of equal energy, for energies between 200 and 400 kev.

The Inelastic Scattering of Very Slow Neutrons by Iron, by R. LATHAM and J. M. CASSELS.

ABSTRACT. The increase with temperature of the total cross section of iron for very slow neutrons has been measured with the help of a cyclotron and a neutron velocity selector. Part at least of this increase is caused by the inelastic scattering associated with lattice vibrations, but the observed rise in cross section is much greater than is predicted by the theory of this effect. It is suggested that a ferromagnetic scattering process may be responsible for the discrepancy.

The Angular Distribution of Scattered Nucleons in High Energy Nuclear Collisions, by H. MESSEL and H. S. GREEN.

ABSTRACT. The theory of the mean square angle of emission of nucleons resulting from a high energy nucleon–nucleus collision is developed. Graphical results are given both for light and for heavy nuclei.

The Nuclear Magnetic Moment of $^{197}_{79}Au$, by F. M. KELLY.

ABSTRACT. The hyperfine structure of the 6s and 7s levels of Au I have been measured. The values of the nuclear magnetic moments calculated from the structure of these two levels using the Goudsmit–Fermi–Segrè formula agree. Since the Fermi–Segrè factor is very large (1·424) for the 6s level and small (1·038) for the 7s level, this affords a good check on the validity of the method introduced by Crawford and Schawlow for the evaluation of this factor. When the corrections for the finite size of the nucleus are included, the spectroscopic value of the nuclear magnetic moment of ^{197}Au is +0·136 n.m.

A Radioactive Isomer of ^{166}Ho, by F. D. S. BUTEMENT.

ABSTRACT. Irradiation of holmium with pile neutrons produces, in addition to 27-hour ^{166}Ho, a new long-lived holmium isotope with a half-life greater than 30 years. It is shown that it cannot be ^{167}Ho produced by neutron capture in ^{166}Ho, nor ^{164}Ho produced by a (n, 2n) reaction. It is therefore probably an isomer of the 27-hour ^{166}Ho.

It decays with emission of β-particle groups of energies 0·18, 0·28 and 1·1 Mev, γ-rays of energies 0·830, 0·725, 0·280, 0·212 and (weak) 0·095 Mev, and weak erbium K x-rays.

β–γ and γ–γ coincidence measurements have been made and a decay scheme suggested.

The Structure of Extensive Showers, by I. D. CAMPBELL and J. R. PRESCOTT.

ABSTRACT. The form of the structure function of extensive showers at small distances from the core has been investigated by observations of coincidences between ionization chambers at sea level.

The observations considered are the decoherence curve and the burst-ratio distribution. Both sets of results indicate a structure function that varies as $1/r^{0\cdot8}$ for small r (less than 0·04 lateral shower units at sea level) as opposed to the well-known Moliere function which behaves as $1/r$ for small r. A modified structure function is given in tabular form. The advantages of the burst-ratio distribution method of studying the structure function are discussed.

Investigations of Atomic and Molecular Absorption Spectra: I—General Features. II—Schumann Region Absorption Spectrum of Gallium Vapour, by W. R. S. GARTON.

ABSTRACT. Previous work on far ultra-violet atomic absorption spectra is summarized and discussed with particular regard to the phenomenon of auto-ionization. Details are given of a current programme of work on line and band absorption spectra of vaporized elements and hydrides, in which special attention is paid to the vacuum ultra-violet. Results for the Schumann region absorption spectrum of Ga vapour are given.

The Ultra-Violet Absorption Spectra of GeO, GeS, GeSe and GeTe, by G. DRUMMOND and R. F. BARROW.

ABSTRACT. The ultra-violet absorption spectra of GeSe and GeTe have been obtained. New band-systems of both molecules have been found, and the vibrational analysis of one of them, the E–X system of GeSe, has been completed. The corresponding system, E–X, of GeS has been considerably extended, and fairly sharp dissociation limits have been found for both GeS and GeSe. A satisfactory spectrogram of GeO in absorption has been obtained. Values of the electronic and vibrational constants for all the known states of the four molecules are derived.

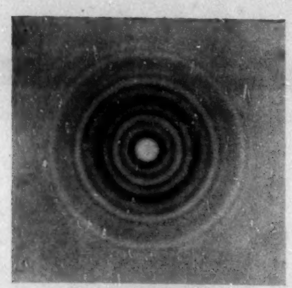

Fig. 2. Diffraction pattern from the model representing benzene, obtained by rotating the original plate during the printing of a diapositive.

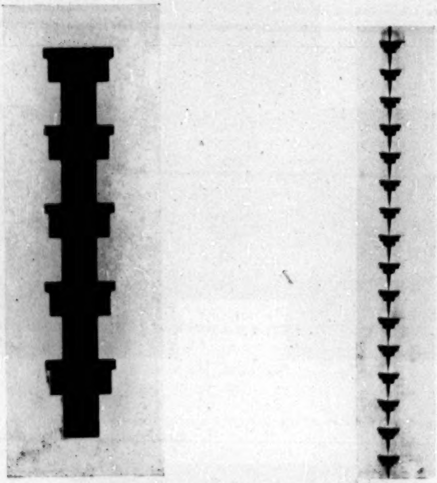

(*a*) (*b*)

Fig. 3. (*a*) Model of benzene formed only with slits. (*b*) Model of benzene formed with slits and wedges.

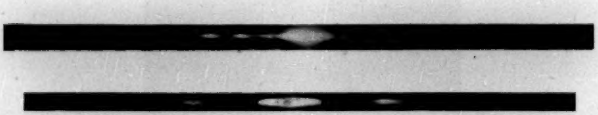

Fig. 5. Diffraction patterns from the two models of benzene.

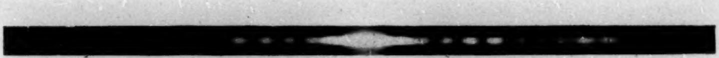

Fig. 6. Diffraction pattern from the model representing CCl_4.

Fig. 7. Model used for CCl_4 in the problem of the radial distribution.

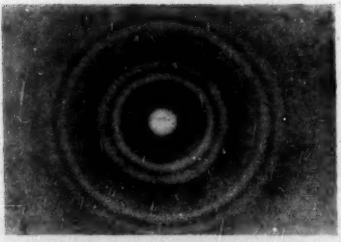

Fig. 8. Rotation diffraction pattern from the model of fig. 7.

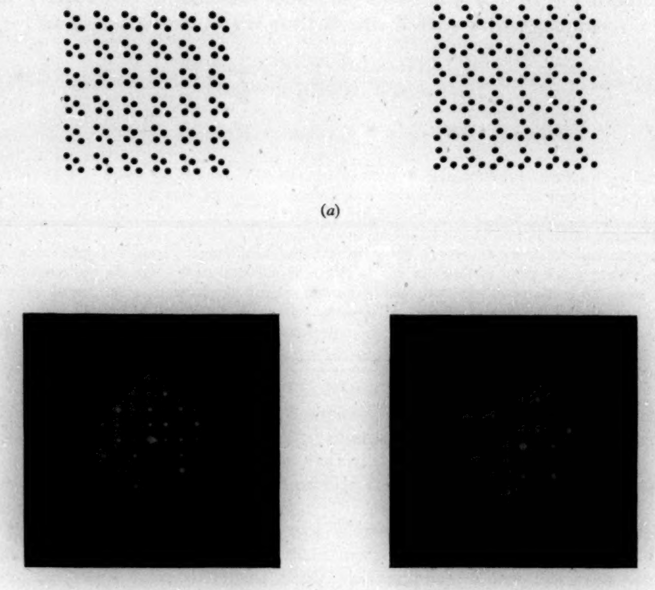

(*a*)

(*b*)

(*a*) Homometric gratings each containing four identical atoms in the elementary parallelogram.
(*b*) Diffraction patterns from these gratings.